A&A 379, 955–975 (2001)
DOI: 10.1051/0004-6361:20011393

Astronomy & Astrophysics

Non-LTE line formation for N I/II: Abundances and stellar parameters

Model atom and first results on BA-type stars⋆

N. Przybilla and K. Butler

Universitäts-Sternwarte München, Scheinerstraße 1, 81679 München, Germany

Received 2 July 2001 / Accepted 20 September 2001

Abstract. A comprehensive model atom for non-LTE line formation calculations for neutral and singly-ionized nitrogen is presented. Highly accurate radiative and collisional atomic data are incorporated, recently determined for astrophysical and fusion research using the R-matrix method in the close-coupling approximation. As a test and first application of the model, nitrogen abundances are determined on the basis of line-blanketed LTE model atmospheres for five stars, the main sequence object Vega (A0 V) and the supergiants η Leo (A0 Ib), HD 111613 (A2 Iabe), HD 92207 (A0 Iae) and β Ori (B8 Iae), using high S/N and high-resolution spectra at visual and near-IR wavelengths. The computed non-LTE line profiles fit the observations excellently for a given nitrogen abundance in each object. Moreover, the ionization equilibrium of N I/II proves to be a sensitive temperature indicator for late B-type and early A-type supergiants – even at low metallicities – due to the apparent nitrogen overabundance in these objects. All supergiants within our sample show an enrichment of nitrogen on the order of ∼0.3–0.6 dex, indicating the mixing of CN-cycled material into atmospheric layers, with the sum of the CNO abundances staying close to solar. This finding is in accordance with recent stellar evolution models accounting for mass-loss and rotation. For Vega, an underabundance of nitrogen by 0.25 dex is found, in good agreement with the similar underabundance of other light elements. The dependence of the non-LTE effects on the atmospheric parameters is discussed with special emphasis on the supergiants where a strong radiation field at low particle densities favours deviations from LTE. Non-LTE effects systematically strengthen the N I/II lines. For some N I lines in supergiants non-LTE abundance corrections in excess of 1 dex are found and they react sensitively to modifications of the collisional excitation data. The influence of microturbulence on the statistical-equilibrium calculations is also investigated: the line-strengths of the strong N I features show some sensitivity due to modifications of the line-formation depths and the departure coefficients, while the – in this parameter range – weak N II lines remain unaffected.

Key words. atomic data – line: formation – stars: abundances, early-type, fundamental parameters, supergiants

1. Introduction

Nitrogen is a key element for the understanding of the evolution of massive stars. Together with carbon and oxygen it is the main catalyst for fusion processes in the stellar interior. These alter the initial abundance ratios of these elements, with the sum of CNO remaining constant, and also enrich helium. Subsequently, the fusion products can be mixed into the atmospheric layers resulting in observable abundance anomalies. The presence of CN-cycle products (the oxygen abundance alters insignificantly) even in some main sequence B-stars is reported by Lyubimkov 1991, and references therein), Gies & Lambert (1992) and Kilian (1992), while for OBA-type supergiants such a signature is well established, in particular for higher-mass objects (Gies & Lambert 1992; Herrero et al. 1992, 1999, 2000; Lennon et al. 1993; Lennon 1994; Venn 1995b; McErlean et al. 1999). A theoretical explanation of the observed abundance patterns has been given recently by stellar evolution calculations which include the effects induced by rotation (Meynet & Maeder 2000; Heger & Langer 2000; Maeder & Meynet 2001). Despite qualitative consistency between the derived abundance ratios and the model predictions, considerable efforts are needed to reduce the (in particular systematic) uncertainties in order to pin down the evolutionary status of single stars, e.g. to distinguish blue-loop objects with first dredge-up abundances from direct evolution from the main sequence with partial mixing.

Send offprint requests to: N. Przybilla,
e-mail: nob@usm.uni-muenchen.de

⋆ Based on observations collected at the European Southern Observatory, Chile (ESO N° 62.H-0176).

Both neutral and singly-ionized nitrogen are known to be affected by non-LTE effects (N I: Takeda 1992, Rentzsch-Holm 1996, Lemke & Venn 1996; N II: Dufton & Hibbert 1981, Becker & Butler 1989). In particular, abundances derived by the N I model atoms seem to be troubled by systematic and comparatively large statistical errors. Recently, important improvements in the determination of accurate atomic data have been achieved, e.g. by the Opacity Project (OP; see Seaton et al. 1994 for a general overview) in the calculation of radiative data. Moreover, detailed electron-impact excitation cross-sections have become available due to the demands of technological applications and fusion research (Frost et al. 1998). The latter are of particular interest, as the former non-LTE studies find a sensitivity of the results to different sets of (approximative) collision data and a discrepancy between abundances from N I lines from the doublets and quartets, which also indicates inappropriate collisional coupling.

Thus a critical reinvestigation, accounting for the improved atomic data, seems appropriate. The aim will be to test the model atom not only on a main sequence object (as usually done on Vega) but also on supergiants, where the tenuous atmospheres favour large mean-free-paths between true absorption processes of photons, thus inducing marked non-LTE effects. Moreover, the expected nitrogen overabundance in the massive objects makes it possible to use the N I/II ionization equilibrium as a temperature indicator for late-B/early-A supergiants, as the N II lines – otherwise absent in these spectral types – also become measurable. Moreover, nitrogen enrichments increase considerably in low-metallicity environments like the SMC, as indicated by observations (Venn 1999) and stellar evolution models (Maeder & Meynet 2001); mixing of chemical elements is more efficient at low metallicity because the metal-poor stars are more compact and therefore have greater angular velocity gradients. Thus the N I/II ionization equilibrium remains useful, while the lines of other indicators fade away at lower abundances.

In addition, analyses of supergiants allow stellar evolution models to be constrained, not only for galactic stars, but also for objects in galactic environments at differing metallicity. High-resolution spectroscopy of such targets has become feasible within the Local Group with 8–10 m class telescopes and modern instrumentation – see Venn (1999) and Venn et al. (2000, 2001) for results on A-type supergiants in the SMC, M 31 and NGC 6822. For supergiants outside the Local Group medium-resolution spectroscopy has already been performed (Bresolin et al. 2001), offering the potential to use the unblended stronger N I lines to obtain valuable information on these objects.

An extensive model atom for N I/II is presented in the next section together with a critical examination of the expected systematic uncertainties. We perform a consistent and simultaneous treatment of both ionization stages for the first time. The results from our non-LTE line-formation computations are discussed in Sect. 3, as is the influence of microturbulence. In the following section, stellar parameters are constrained applying the N I/II ionization equilibrium as a temperature indicator and nitrogen abundances are determined for a test sample of five stars using high S/N and high-resolution spectra. The findings are discussed in the context of previous abundance studies. Finally, a short summary is given in Sect. 5.

The implications of the observed nitrogen abundances, and also those of helium, carbon and oxygen, on the evolutionary status of the sample supergiants will be discussed in detail elsewhere (Przybilla et al. 2001b, hereinafter Paper IV). A comparison of our model predictions with observed N I lines in later spectral types (in particular for the sun) and with N II lines in earlier B stars, at maximum strength, would also be of interest.

2. Model calculations

2.1. Model atmospheres and programs

The calculations are performed using the standard assumptions of plane-parallel, homogeneous and stationary stellar atmospheres in hydrostatic and radiative equilibrium. Nitrogen is assumed to be a trace element despite its comparatively large abundance. Its contribution to the continuous opacity is small, as the N I ground state ionization threshold coincides with the overwhelming Lyman continuum and the N II threshold is situated at a frequency where the flux is negligible. Thus, we obtain statistical equilibrium populations for N I/II while keeping the atmospheric parameters fixed.

The non-LTE N I/II line profiles are computed on the basis of ATLAS9 (Kurucz 1979, 1991) LTE line-blanketed model atmospheres using LTE Opacity Distribution Functions (ODFs, Kurucz 1992) to account for line blocking in the spectrum synthesis. For the calculation of model atmospheres for the most extreme supergiants close to the Eddington limit, modifications in the treatment of the opacities in the outermost atmospheric layers become necessary, see Przybilla et al. (2001c; hereinafter Paper III) for details.

With the above assumptions reliable analyses can be performed in the given temperature range from main sequence stars through to bright giants as indicated by Kudritzki (1988). A thorough discussion of the possible deviations from the standard assumptions on the model atmosphere structure of supergiants is given by Venn (1995a). Additionally, non-LTE effects are often less significant for the model structure than is line blanketing, as demonstrated by Przybilla (1997). Close to the Eddington limit (luminosity classes Iae and Ia$^+$) further studies on this topic are desirable; appropriate stellar atmosphere models including non-LTE blanketing, spherical extension and the hydrodynamics of stellar winds are still in the development phase and are not available for detailed abundance studies yet.

The line formation calculations are performed using the programs DETAIL and SURFACE (Giddings 1981; Butler & Giddings 1985), with the former solving the

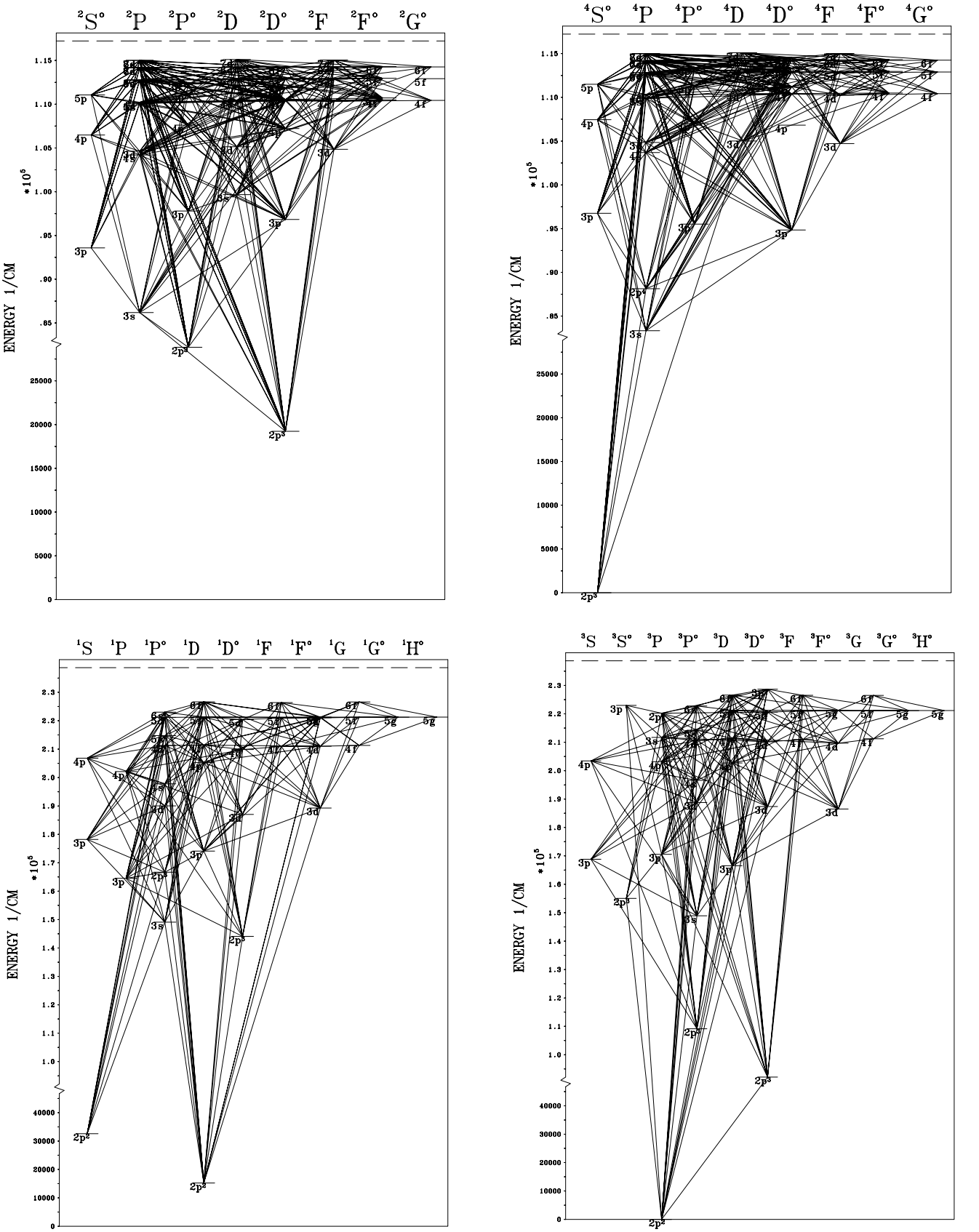

Fig. 1. Grotrian diagrams for N I, doublet (upper left) and quartet spin system (upper right) and for N II, singlets (lower left) and triplets (lower right). Note that both ionic species and all spin systems (with five additional quintet levels in N II) are treated simultaneously. Displayed are the energy levels and the radiative transitions treated explicitly in non-LTE. Numerous intercombination lines, connecting the spin systems of each of the two ionic species, are not shown in the diagram.

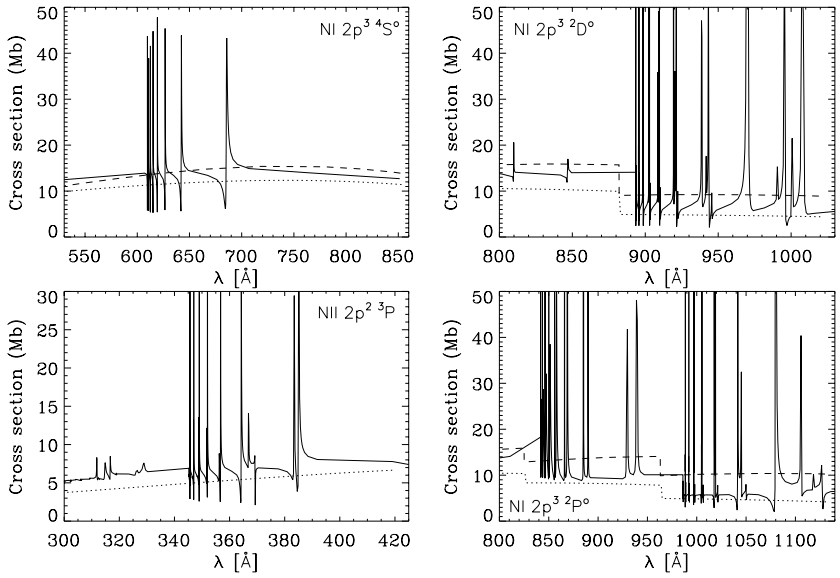

Fig. 2. Comparison of photoionization cross-sections from OP computations (full line) and from Henry (1970, dotted line) and Hofsäß (1979, dashed line). On the left hand side data for the ground states of N I and N II are displayed, on the right hand side data for the first and second excited levels of N I. In general, the cross-sections agree well except for numerous narrow resonances present in the OP computations.

radiative transfer and the statistical equilibrium equations and the latter computing the emergent flux. Recent improvements as the inclusion of an ALI scheme (using the treatment of Rybicki & Hummer 1991) allow the utilisation of quite elaborate model atoms while the necessary computational resources remain at a low level (typically ∼20 min for model convergence on a 1.5 GHz PIV CPU).

2.2. The model atom

2.2.1. Energy levels

The atomic model for nitrogen has to be fairly complete in order to predict the non-LTE effects quantitatively and consequently to ensure that the ionization balance between the atomic and singly-ionized species is accurate. For the most part, nitrogen is singly-ionized throughout the atmosphere of BA-type supergiants, with a fraction of N I on the order of several percent at line-formation depths, rapidly decreasing with increasing temperature. In main sequence stars, this ionization balance is shifted towards the neutral species. Non-LTE effects are expected to be of importance for the interpretation of the N I/II lines at visual and near-IR wavelengths which all emerge from highly-excited levels ($\gtrsim$10.3/18.5 eV above the ground states of N I/II).

Energy levels up to ∼0.26/1.10 eV below the ionization thresholds at 14.53/29.60 eV are therefore explicitly included in our N I/II model as listed by Moore (1993). This includes all observed energy levels with principal quantum number $n \leq 7$ and the 8s states in N I and all observed levels with $n \leq 6$ in N II. Only the ground state of N III is considered as the ionization energy of 47.45 eV is rather high. Fine structure splitting is not taken into account: sub-levels belonging to the same term are combined into a single level. The intermediate coupling terms of N I and N II are split to resemble the LS-coupling levels for which OP radiative data is available. The resulting inconsistencies are expected to be negligible as the deviations from pure LS-coupling are small.

Additionally, the remaining level populations of N I and N II up to $n = 10$ are computed in LTE relative to the ground state of the higher ionization stage with energies derived from their quantum defects. They are considered only in the number conservation equation.

2.2.2. Radiative transitions

All optically allowed bound-bound transitions between energy levels with non-LTE populations are taken into consideration. The oscillator strengths required are OP data (Burke & Lennon, available only from the TOPBASE database Cunto & Mendoza 1992) for N I and from Luo & Pradhan (1989) for N II. In order to improve the computational efficiency the individual lines of a multiplet are reduced to a single effective "multiplet line".

Grotrian diagrams for N I and N II are displayed in Fig. 1. The non-LTE calculations are performed simultaneously for N I/II. Additional radiative coupling between the different spin systems of N I/II is provided by the intercombination transitions listed by Wiese et al. (1996). A detailed comparison of OP oscillator strengths for N II with experimental and theoretical work by other authors is performed by Luo & Pradhan (1989); considerable disagreement for a number of transitions is found. Nevertheless, the superior performance of the *R*-matrix method in the close-coupling approximation typically allows the determination of atomic data accurate to within 10%. We therefore expect the uncertainties of the majority of the data to remain within this limit, outdating most of the older data used in previous studies on non-LTE effects in N I or N II.

Photoionization from all energy levels with non-LTE populations are treated with cross-sections fitted to the OP data (Burke & Lennon, available only from the TOPBASE database) for N I and from Luo & Pradhan (1989) for N II. A carefully chosen frequency grid ensures

a thorough representation of the numerous resonances present in the results of the R-matrix calculations, typically being accurate to 10%. Cross-sections for energy levels missing in the OP data (for quantum number $\ell = 4$ in N I) are calculated in the hydrogenic approximation (Mihalas 1978, p. 99).

A comparison of OP cross-sections for the ground states and some low-excitation levels with those of Henry (1970) and Hofsäß (1979) – used in previous non-LTE studies on N I/II – is given in Fig. 2. All three show the same general trend and agree well to a factor better than 2, except for the numerous narrow resonances present in the OP data. For the higher-excited levels of N I/II the use of detailed OP data also significantly improves the description of the photoionization processes compared to the majority of previous non-LTE studies of those ions.

In the first step of the computations, i.e. in DETAIL, the level populations are calculated using depth dependent Doppler profiles assuming LS coupling; microturbulence is explicitly accounted for by inclusion of an additional term in the Doppler width ($\Delta\lambda_{\rm D}$):

$$\Delta\lambda_{\rm D} = \frac{\lambda_0}{c}\sqrt{v_{\rm th}^2 + \xi^2} \qquad (1)$$

where λ_0 is the rest wavelength of the transition, c the speed of light, $v_{\rm th}$ the thermal velocity for the chemical species of interest and ξ the microturbulent velocity; see Sect. 3.2 for a discussion. Both continuous opacities and ATLAS9 line-distribution functions are accounted for in solving the radiation transfer.

These LS-coupling populations are then split according to the statistical weights of the individual sub-levels in order to calculate line profiles via the program SURFACE. In this step Voigt profile functions are adopted and the same microturbulent velocity as in DETAIL is applied. The damping parameters are calculated from OP radiative lifetimes for the radiative widths and adopted from Griem (1964, 1974) for electron impact and ion broadening in N I/II. Missing collisional damping data are computed from the approximation of Cowley (1971). Van der Waals damping is neglected, as the atmospheric plasma is almost completely ionized in the parameter range considered here.

2.2.3. Collisional transitions

The interest in accurate collisional excitation data for N I/II in technological applications and fusion-plasma modelling has led to significant progress in computations and measurements for this kind of data recently. Frost et al. (1998) have performed R-matrix calculations for electron-impact excitations in N I/II for all transitions involving energy levels with principal quantum numbers $n \leq 3$. Therefore, for a significant fraction (over 450 transitions) – also the most important – of the data needed in our work, accurate temperature-dependent effective collision strengths are available. The authors find agreement of their computed data and their measurements for selected

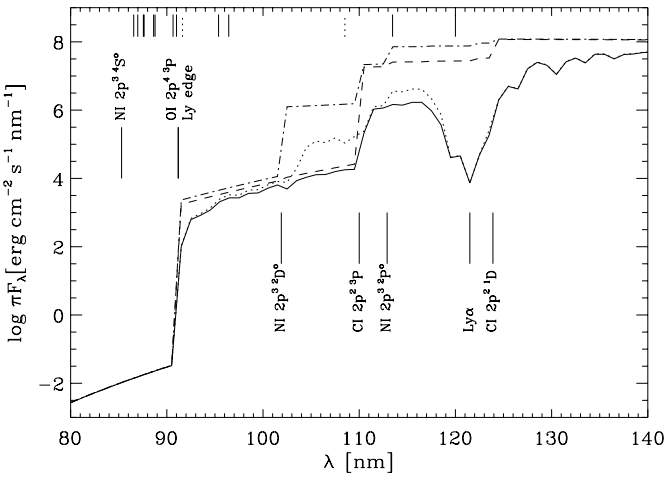

Fig. 3. Synthetic far-UV (astrophysical) fluxes from ATLAS9 supergiant models for $T_{\rm eff}$ = 9500 K, $\log g$ = 2.0 and ξ = 4 km s^{-1} at solar metallicity, accounting for continuous and (ODF) line opacity (full/dotted line) and continuous opacity only (dashed/dashed-dotted line) for solar/0.2 × solar carbon abundance and a correspondingly increased nitrogen abundance in the latter case. The locations of the relevant ionization edges and Ly$_\alpha$ are marked; continuous and dotted markers on the top give the positions of the resonance lines of N I and N II, respectively (Wiese et al. 1996).

transitions within a factor of generally ∼2, with a few transitions discrepant up to a factor of 10. For the remaining bulk of the transitions, approximate formulae must be used, giving threshold values accurate to a factor 2-3 at best. Van Regemorter's formula (Van Regemorter 1962) is applied for radiatively permitted transitions with OP oscillator strengths and for the optically forbidden transitions, the semiempirical Allen formula (Allen 1973) is used with the collision strength Ω set to 1.0. For collisions between the (artifically split) LS-coupling states belonging to the same intermediate-coupling level, we set $\Omega = 1000$ in these energetically close levels to enforce their coupling.

Experimental cross-sections from Brook et al. (1978) and Yamada et al. (1989) are adopted for the collisional ionization of the ground states of N I and N II. The authors expect uncertainties <40% and <20%, respectively, for the data at low energies, with significant improvements in the accuracy at higher energies. All the remaining collisional ionization data are computed using the Seaton formula (Seaton 1962) with threshold photoionization cross-sections from the OP data, where available, or from the hydrogenic approximation.

2.3. Background opacities

The stellar radiation field is strongly affected by continuous and line opacities which must be correctly accounted for in the statistical equilibrium calculations. Synthetic (ATLAS9) far-UV fluxes for typical supergiant parameters are displayed in Fig. 3 for two sets of C and N abundances, together with the locations of the relevant opacity

sources (ionization edges) and N I/II resonance lines in this wavelength region. The coarse wavelength resolution of the flux results from the 10 Å-wide ODF bins. Ionization from the C I ground state is an important opacity source in the solar abundances model, next to the line opacity. Its rôle diminishes for a carbon depleted (by a factor of five) model; here, the enhanced bound-free opacity from the first excited level of N I almost replaces it, except for the region between these two ionization edges. We assume that the depleted carbon is transformed into nitrogen, as might be expected if CN-cycled matter is mixed into the atmospheric layers. This LTE experiment should be viewed only as an instructive example for the effects anticipated, as a fully consistent treatment in non-LTE is beyond the scope of this work, see also the remarks at the end of this section.

We therefore explicitly include bound-free opacities for H , He , O and C with level populations calculated in non-LTE, using updated and extended versions of the H and He I model atoms of Husfeld et al. (1989) and the model atoms of Przybilla et al. (2000, hereinafter Paper I; Paper III). All levels of H up to $n = 20$ are treated explicitly in non-LTE, and for He I a number of spectral lines is added in the line formation; however, the changes do not affect the contribution of both elements to the background opacity.

Line opacities are represented by LTE ODFs (Kurucz 1992) for the appropriate metallicity and microturbulence. The original sawtooth pattern is transformed into a step function by averaging over the 10 Å-wide intervals. This procedure meets the requirements for calculating the radiation field as a whole. However, at certain important wavelengths a more detailed description is desirable. In particular, line opacities slightly longward of the Lyman and Balmer jump are only poorly reproduced in the ODF approach, especially for supergiants, as the merging hydrogen lines are inappropriately sampled. Moreover, most transition wavelengths for opacity calculations are only known from theoretical calculations which implies comparatively large errors (see e.g. Johansson & Leckrone 1996) and therefore less accurate opacities. In particular, the vacuum ultraviolet region is affected, where the ionization edges of the first and second excited levels of N I are located. Fortunately, the ionization of the N I ground state is determined by the optically thick Lyman continuum and N II has its ionization edges located at wavelengths with negligible flux.

Despite our success in reproducing the observations, our calculations might also be affected by a systematic effect neglected in the atmosphere modelling. Non-LTE effects will cause an overionization of the relevant elements in the opacity determination. The backwarming introduced by line blanketing might therefore be overestimated in LTE, as well as the magnitude of line blocking. First calculations of non-LTE line-blanketed model atmospheres for main sequence A-types (Hubeny & Lanz 1993) indicate some changes in the expected direction but adequate models for the more interesting case of supergiants are just being investigated (J. Puls, private communication, Aufdenberg 2000) and are still not available for detailed abundance work.

2.4. Error estimates for the nitrogen non-LTE calculations

To assess the effects of uncertainties in the atmospheric parameters and crucial atomic data on the accuracy of our non-LTE computations, test calculations were performed for typical atmospheric parameters of BA-type stars: a main sequence model with 9500 K/4.0 ($T_{\rm eff}/\log g$) at $\xi = 2\,{\rm km\,s^{-1}}$ and supergiant models with 9500 K/2.0 at $\xi = 4\,{\rm km\,s^{-1}}$ and with 9500 K/1.2 and 12 000 K/1.8 at $\xi = 8\,{\rm km\,s^{-1}}$, assuming solar metallicity. For each parameter or set of cross-sections varied, we calculated a small grid at different abundances to investigate the systematic shift in abundance needed to fit the original line strengths. The results of the tests are summarised in Table 1. They correspond to the mean value obtained from a study of the lines $\lambda\lambda$ 6008, 7423, 7468, 7899, 8567, 8629, 8680, 8686, 8711, 8718, 9028, 9045 (N I) and λ 3995 (N II, for $T_{\rm eff} < 10\,000$ K) and $\lambda\lambda$ 3995, 4447, 4613, 4630, 4788, 5045, 5679, 5686 (N II, for $T_{\rm eff} > 10\,000$ K).

The strengths of the N I and/or N II lines are highly dependent on the atmospheric parameters ($T_{\rm eff}/\log g$). This sensitivity predestines the ionization equilibrium of N I/II as an ideal tool for the determination of stellar parameters in BA-type supergiants (N II lines are absent in the corresponding main-sequence objects). A modification of the stellar helium content affects the atmospheric structure (Kudritzki 1973) and considerable enrichment is expected for supergiants (e.g. Meynet & Maeder 2000). We therefore examine the effects of an increased helium abundance (by a typically amount) on the nitrogen lines: in some cases this consitutes one of the more important contributors to systematic errors while in others it is completely negligible. In the following estimation of the systematic error we ignore this effect as we explicitly determine the helium abundance and account for it in the model atmosphere computations; unfortunately, this is not being done in most of similar studies found in the literature. The other atmospheric and stellar parameters like microturbulence and metallicity are almost negligible and affect only the strongest features. In particular, no dependency of the nitrogen ionization equilibrium on reasonable uncertainties in the carbon abundance is found. Carbon affects the radiation field in the far-UV due to the bound-free absorption from the C I ground state shortward of 1100 Å. But, line opacity in general is found to be of greater importance for the ionization from excited N I levels, while photoionizations from the N I ground state arise under optically thick conditions (in the Lyman continuum), which implies small deviations from LTE.

The accuracy of the atomic data used in the model is high and variations within the uncertainties result in negligible abundance errors in most cases. In general, the gf-values for the visible N I/II lines are well determined,

Table 1. Uncertainties in the non-LTE analysis of nitrogen.

		changes in $\log \varepsilon(\mathrm{N})_{\mathrm{NLTE}}$						
		9500/4.0	9500/2.0		9500/1.2		12 000/1.8	
		N I	N I	N II	N I	N II	N I	N II
Atmospheric parameters:								
$T_{\rm eff}$ − 150 K	$\sigma_{T_{\rm eff}}$	−0.02	−0.04	+0.11	−0.06	+0.09	−0.02	+0.08
$\log g + 0.15$ dex	$\sigma_{\log g}$	+0.04	−0.01	+0.10	−0.11	−0.04	−0.04	+0.12
ξ +1 km s^{-1}	σ_{ξ}	−0.02	−0.01	−0.02	±0.00	±0.00	±0.00	±0.00
$y + 0.15$ dex		+0.02	−0.02	±0.00	−0.03	+0.01	±0.00	−0.06
[M/H] − 0.2 dex	$\sigma_{\rm [M/H]}$	±0.00	±0.00	+0.01	−0.02	−0.01	±0.00	±0.00
[C/H] − 0.2 dex	$\sigma_{\rm [C/H]}$	±0.00	±0.00	±0.00	±0.00	±0.00	±0.00	±0.00
Line transitions:								
Oscillator strengths +10%	$\sigma_{\log gf}$	−0.05	−0.04	−0.04	−0.04	−0.05	−0.04	−0.04
Damping constant ∗2	$\sigma_{\rm damp}$	±0.00	±0.00	±0.00	±0.00	±0.00	±0.00	±0.00
Photoionisations:								
Cross-sections +10%	$\sigma_{\rm rbf}$	±0.00	±0.00	±0.00	±0.00	±0.00	±0.00	±0.00
Cross-sections ∗5		+0.01	+0.04	±0.00	+0.03	±0.00	+0.05	±0.00
Collisional transitions:								
Cross-sections ∗0.1		−0.30	−0.06	−0.02	−0.01	−0.01	−0.05	−0.03
Cross-sections ∗0.5	$\sigma_{\rm cbb}$	−0.11	−0.03	−0.01	±0.00	−0.01	−0.02	−0.01
Cross-sections ∗2	$\sigma_{\rm cbb}$	+0.09	+0.05	+0.01	+0.01	+0.01	+0.02	+0.02
Cross-sections ∗10		+0.23	+0.22	+0.07	+0.06	+0.05	+0.13	+0.09
Collisional ionization:								
Cross-sections ∗0.1	$\sigma_{\rm cbf}$	+0.01	+0.01	±0.00	±0.00	±0.00	±0.00	±0.00
Cross-sections ∗10	$\sigma_{\rm cbf}$	−0.01	−0.01	+0.01	±0.00	±0.00	±0.00	±0.00
Continuum placement	$\sigma_{\rm cont}$	±0.05	±0.05	±0.05	±0.05	±0.05	±0.05	±0.05
Estimated total uncertainty	$\sigma_{\rm sys}$	±0.14	±0.09	±0.16	±0.14	±0.12	±0.08	±0.16

with typical uncertainties in the 10% range, cf. Tables 5 and 6. Although small, these consitute the main source of (atomic data) systematic error for supergiant analyses (up to 0.05 dex). Variations of the photoionization cross-sections within the expected 10% on the other hand result in no abundance changes. This is in contrast to some of the previous non-LTE studies, for which only less accurate data were available. Also, the damping constants are not a critical issue in the line-formation. Collisional ionization from the energetically low-lying energy levels is unimportant due to the fairly low kinetic energy of the electrons (∼1 eV) as compared to the ionization energies of 14.53 and 29.60 eV for N I and N II, respectively. For the high-excitation levels this processes ensure the coupling to the next ionization stage, but changes by a factor 10 in the rates do not affect the visible lines.

The other critical parameters for the non-LTE analysis besides the gf-values are the collisional excitation data, see also Rentzsch-Holm (1996). This is clearly demonstrated for the main-sequence model, where a systematic uncertainty in the rates within a factor of two results in an abundance differing by 0.1 dex. A factor of 10, which is easily reached for isolated transitions – if the detailed computations of Frost et al. (1998) are compared with the approximative formula commonly used – will lead to abundances differing by up to 0.3 dex in the mean. For single lines, like N I λ8680, the abundance can be modified by even 0.5 dex. Naturally, the resulting errors diminish for supergiants as collisions become less important in their tenuous atmospheres. Nevertheless, we identify the usage of the detailed collisional excitation data as the main improvement in our non-LTE analysis as compared to previous studies, in particular for N I; consistent results from spectral lines of the doublets and quartets are obtained for the first time (cf. Sect. 4.3).

A further source of systematic error is the continuum placement in the observed spectra. This strongly depends on the S/N ratio obtained. Our estimate in Table 1 should be applicable to high quality data with $S/N \gtrsim 100$ only. In general, equivalent widths studies are more susceptible to this systematic error than the spectrum synthesis technique, which also accounts for the continuum regions explicitly.

The total uncertainties are computed from the sum of the squares of the appropriate uncertainties listed above, assuming them to be independent:

$$\sigma^2_{\rm sys} = \sigma^2_{T_{\rm eff}} + \sigma^2_{\log g} + \sigma^2_{\xi} + \sigma^2_{\rm [M/H]} + \sigma^2_{\rm [C/H]} + \sigma^2_{\log gf} + \sigma^2_{\rm damp} + \sigma^2_{\rm rbf} + \sigma^2_{\rm cbb} + \sigma^2_{\rm cbf} + \sigma^2_{\rm cont}. \quad (2)$$

The systematic error of abundance determinations for nitrogen *within* our methodology (cf. Sect. 2.1) is therefore typically 0.15 dex in main sequence stars and supergiants alike, but with differing error sources. Under main sequence conditions the uncertainties in the collisional excitation data dominate, while for supergiants the main uncertainties arise from inaccurate stellar parameters.

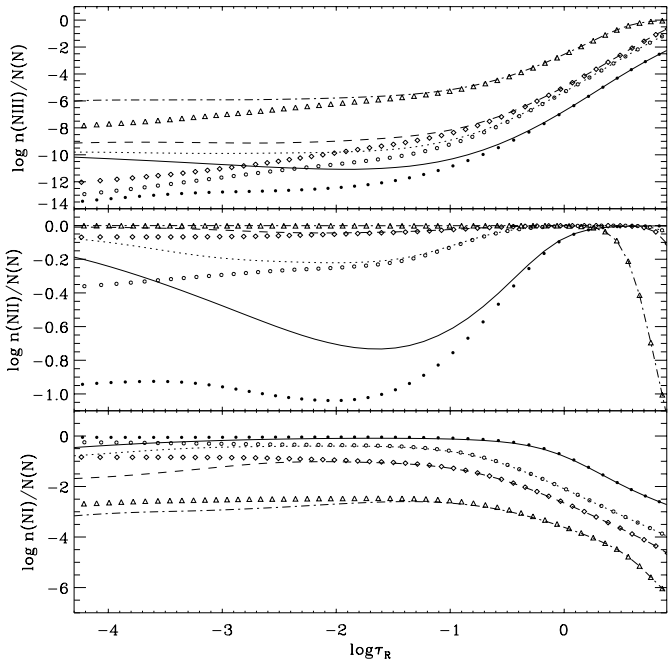

Fig. 4. Non-LTE and LTE ionization balance of nitrogen for several sample stars of Sect. 4: Vega (solid lines and filled circles, respectively), η Leo (dotted lines/open circles), HD 92207 (dashed lines/open diamonds) and β Ori (dashed-dotted lines/open triangles). Displayed are the ratios of the total level populations of the three ionization stages n(N I/II/III) to the total nitrogen population N(N) as a function of Rosseland optical depth $\tau_{\rm R}$.

3. Discussion

In this section we evaluate the advantages of time-consuming non-LTE calculations over a straightforward LTE analysis for the interpretation of the N I/II spectra of BA-type stars. The nature of the non-LTE effects is discussed for the stars of our test sample in Sect. 4. Next, the influence of the microturbulence parameter on the line formation calculations is studied. Finally, our results are compared with those of previous studies of non-LTE effects in nitrogen.

3.1. The non-LTE effects

The run of the ionization fractions of N I–III with Rosseland optical depth $\tau_{\rm R}$ in the photospheres of several stars from our sample is displayed in Fig. 4. For the early A-type main sequence star, nitrogen remains neutral throughout most of the atmosphere with N II becoming dominant for $\tau_{\rm R} \gtrsim 1$ and with a negligible fraction of N III. This picture changes drastically in the early A-type supergiants, where nitrogen is almost entirely singly-ionized in the photosphere and the N I fraction drops to the percent level. The N III fraction – although enhanced – is still insignificant at line-formation depths. In the late-B supergiant N I diminishes further to several parts in ten-thousand at line-formation depths, while N III rapidly becomes the dominant ionization stage below the continuum formation region. The tenuous atmospheres of the supergiants faciliate ionization processes through large mean-free paths for the photons of the rapidly intensifying

Table 2. Term identifiers.

Ion	No.	Term	Ion	No.	Term	Ion	No.	Term
N I	1	$2p^3\ ^4S^o$	N I	13	$3s'\ ^2D$	N II	97	$3s\ ^3P^o$
	2	$2p^3\ ^2D^o$		16	$3d\ ^2P$		98	$3s\ ^1P^o$
	3	$2p^3\ ^2P^o$		30	$4d\ ^2P$		100	$3p\ ^1P$
	4	$3s\ ^4P$		43	$3p'\ ^2F^o$		101	$3p\ ^3D$
	5	$3s\ ^2P$		50	$3p'\ ^2P^o$		103	$3p\ ^3S$
	7	$3p\ ^2S^o$	N II	90	$2p^2\ ^3P$		104	$3p\ ^3P$
	8	$3p\ ^4D^o$		91	$2p^2\ ^1D$		105	$3p\ ^1D$
	10	$3p\ ^4S^o$		92	$2p^2\ ^1S$		108	$3d\ ^1D^o$
	12	$3p\ ^2P^o$		93	$2p^3\ ^5S^o$		109	$3d\ ^3D^o$
						N III	167	$2p\ ^2P^o$

Table 3. Line identification.

Ion	λ (Å)	Transition	l–u
N I	3830.43	$3s\ ^2P-3p'\ ^2P^o$	5–50
	5999.43	$3p\ ^2S^o-4d\ ^2P$	7–30
	6008.47	$3p\ ^2S^o-4d\ ^2P$	7–30
	7423.64	$3s\ ^4P-3p\ ^4S^o$	4–10
	7442.30	$3s\ ^4P-3p\ ^4S^o$	4–10
	7468.31	$3s\ ^4P-3p\ ^4S^o$	4–10
	7898.98	$3s'\ ^2D-3p'\ ^2P^o$	13–50
	7899.28	$3s'\ ^2D-3p'\ ^2P^o$	13–50
	8567.74	$3s\ ^2P-3p\ ^2P^o$	5–12
	8594.00	$3s\ ^2P-3p\ ^2P^o$	5–12
	8629.24	$3s\ ^2P-3p\ ^2P^o$	5–12
	8655.88	$3s\ ^2P-3p\ ^2P^o$	5–12
	8680.28	$3s\ ^4P-3p\ ^4D^o$	4–8
	8683.40	$3s\ ^4P-3p\ ^4D^o$	4–8
	8686.15	$3s\ ^4P-3p\ ^4D^o$	4–8
	8703.25	$3s\ ^4P-3p\ ^4D^o$	4–8
	8711.70	$3s\ ^4P-3p\ ^4D^o$	4–8
	8718.84	$3s\ ^4P-3p\ ^4D^o$	4–8
	8728.90	$3s\ ^4P-3p\ ^4D^o$	4–8
	9028.92	$3p\ ^2S^o-3d\ ^2P$	7–16
	9045.88	$3s'\ ^2D-3p'\ ^2F^o$	13–43
	9049.49	$3s'\ ^2D-3p'\ ^2F^o$	13–43
	9049.89	$3s'\ ^2D-3p'\ ^2F^o$	13–43
N II	3955.85	$3s\ ^3P^o-3p\ ^1D$	97–105
	3995.00	$3s\ ^1P^o-3p\ ^1D$	98–105
	4447.03	$3p\ ^1P-3d\ ^1D^o$	100–108
	4601.48	$3s\ ^3P^o-3p\ ^3P$	97–104
	4607.15	$3s\ ^3P^o-3p\ ^3P$	97–104
	4613.87	$3s\ ^3P^o-3p\ ^3P$	97–104
	4630.54	$3s\ ^3P^o-3p\ ^3P$	97–104
	4643.09	$3s\ ^3P^o-3p\ ^3P$	97–104
	4788.14	$3p\ ^3D-3d\ ^3D^o$	101–109
	4803.29	$3p\ ^3D-3d\ ^3D^o$	101–109
	5045.10	$3s\ ^3P^o-3p\ ^3S$	97–103
	5666.63	$3s\ ^3P^o-3p\ ^3D$	97–101
	5676.02	$3s\ ^3P^o-3p\ ^3D$	97–101
	5679.56	$3s\ ^3P^o-3p\ ^3D$	97–101
	5686.21	$3s\ ^3P^o-3p\ ^3D$	97–101
	5710.77	$3s\ ^3P^o-3p\ ^3D$	97–101

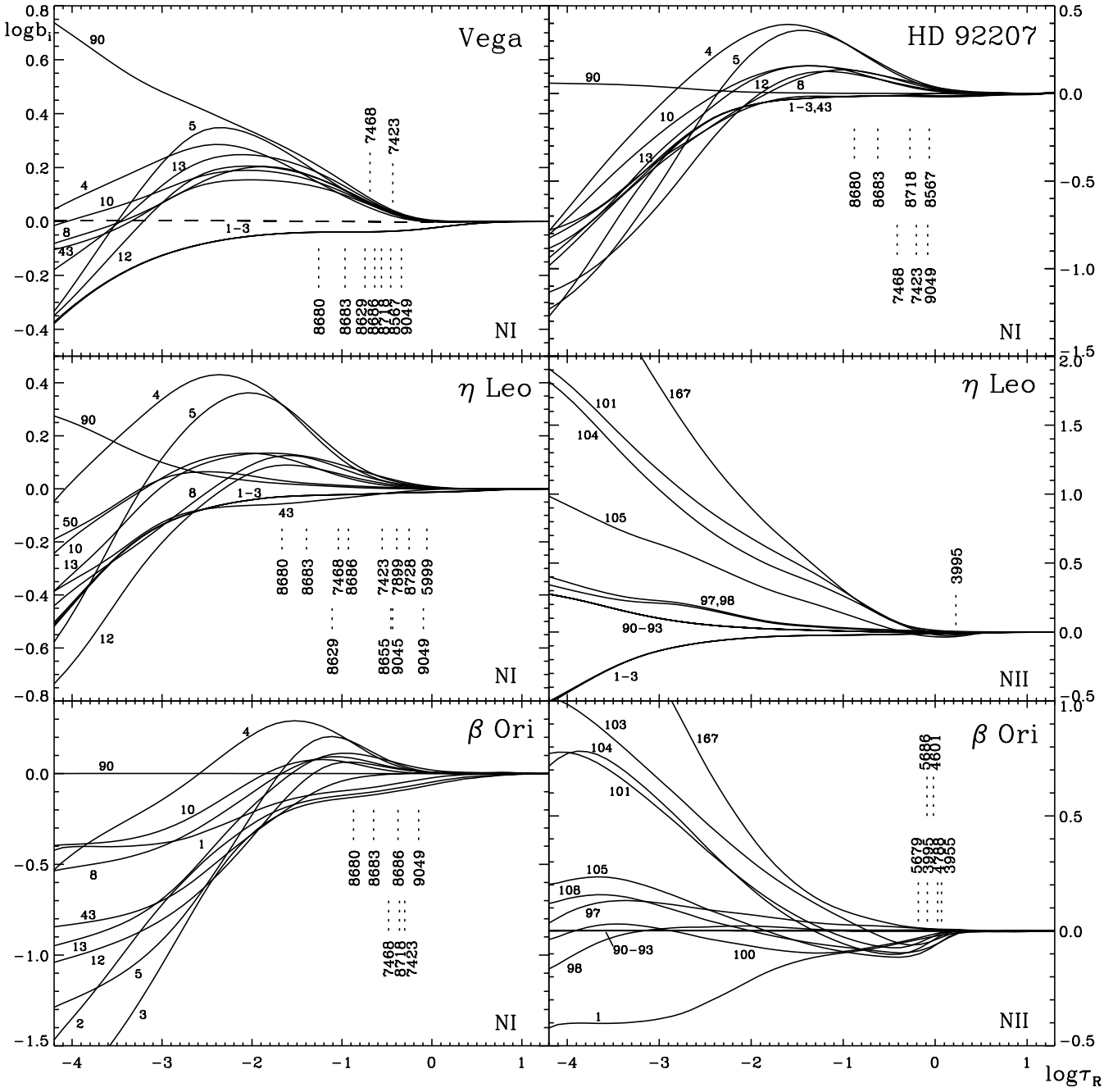

Fig. 5. Departure coefficients b_i for N I/II as a function of Rosseland optical depth $\tau_{\rm R}$ for several of the sample stars of Sect. 4. The formation depths of the line cores ($\tau \approx 1$) for several transitions are indicated. Term identifiers and the levels involved in the transitions are found in Tables 2 and 3. For the Vega model, the departure coefficients for the lowest three levels of N I are also shown after setting $J_\nu = B_\nu$ for the photoionization continua (dashed line). N II lines are absent in the Vega spectrum, the departure coefficients for that ion in HD 92207 behave qualitatively similar to those in η Leo.

(with $T_{\rm eff}$) radiation field. Non-LTE effects favour the overionization of N I and result in an overpopulation of the ionized species.

Departure coefficients $b_i = n_i^{\rm NLTE}/n_i^{\rm LTE}$ (the n_i denoting the level populations) for energy levels i are displayed in Fig. 5 as a function of $\tau_{\rm R}$ for some models of the objects discussed in Sect. 4. All the observed N I/II lines in the visual/near-IR originate from highly-excited energy levels ($\gtrsim$10.3/18.5 eV); the formation depths (at $\tau \approx 1$) of the line cores are also marked in Fig. 5. In Table 2, identifiers for the consecutively numbered energy terms of our N I/II model are given and the levels involved in the observed transitions are identified in Table 3.

Deep in the atmosphere, the departure coefficients approach unity, as the density increases and collisional processes dominate, enforcing LTE (inner boundary condition). Farther out, non-LTE effects prevail and affect the level populations throughout the bulk of the photosphere. A remarkable feature of the departure coefficients for the levels in N I is the separation of the energetically close

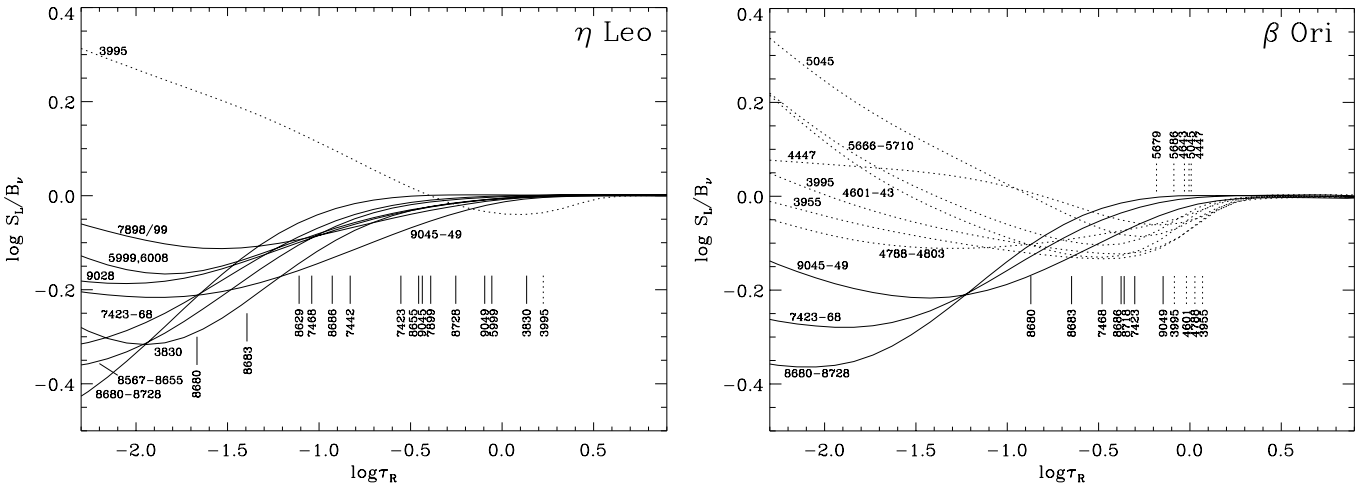

Fig. 6. Ratio of line source function $S_{\rm L}$ to Planck function B_ν at line centre for diagnostic lines of N I (full lines) and N II (dotted lines) as a function of $\tau_{\rm R}$ for our models of η Leo (left) and β Ori (right). The formation depths of the line cores ($\tau \approx 1$) are indicated.

ground state and the collisionally coupled first two doublet levels from the rest of the highly-excited levels. The energetically lowest levels are depopulated by photoionizations: when we neglect the non-LTE radiation field by replacing the mean intensity by the Planck function, $J_\nu = B_\nu$, in the photoionization continua, this situation is relaxed and these levels stay at their detailed-equilibrium value, as a test on Vega has shown (cf. Fig. 5). Photoionizations are mainly effective for the two doublet terms, as the optically thick Lyman continuum blocks the photons necessary for ground state ionization. This overionization of N I is accompanied by a corresponding overpopulation of the N II ground state (and also the collisionally coupled low-lying N II levels). Accurate photoionization cross-sections are therefore necessary to predict the N I/II ionization equilibrium in non-LTE quantitatively, given the small contribution of all other N I energy levels to the total of neutral nitrogen. In the β Ori model, the collisional coupling of the low-excitation levels is weakened, as radiative processes are more intense in the hotter atmosphere.

The higher-excited levels of N I on the other hand develop considerable overpopulations in the line-formation region, most notably for the lower levels of the strongest N I lines in the near-IR, $3s\,^4P$ and $3s\,^2P$. A marked non-LTE strengthening of this lines is therefore expected. The overpopulation reaches a maximum at $-2.5 \lesssim \log \tau_{\rm R} \lesssim -1$ in the various models. Farther out in the atmosphere the trend is reversed and the departure coefficients approach the underpopulation of the low-excitation states. The overpopulation is faciliated by radiative cascades, which in both spin systems of N I practically end in the 3s states. Effectively, these states become metastable, as the transitions to the $2p^3$ levels are optically thick and consequently contribute only marginally to the depopulation of these levels. The radiative detailed balance begins to break down for the $2p^3\ ^2D^o$–$3s\ ^2P$ and $2p^3\ ^2P^o$–$3s\ ^2P$ transitions in the most luminous objects of our sample, weakening the quasi-metastable character of the $3s\ ^2P$ level in these stars. This effect was first identified by Takeda & Takada-Hidai (1995), who also found that it critically depends on the computational details. Our more sophisticated modelling largely improves the agreement between theory and observation, but good quantitative agreement is still not obtained (see Sect. 4.3). Closer to the stellar surface the lower particle densities complicate the recombination and thus the cascading is suppressed. Departure coefficients for levels at slightly higher excitation energy (the other levels with $n = 3$) follow this trend to a lesser degree (these are the upper states for the observed transitions), while the levels close to the N I continuum approach the departure coefficient of the N II ground state, as collisional coupling becomes significant.

As N II becomes the dominant ionization stage, like in the more luminous supergiants, the (triplet) ground state departure coefficient approaches its detailed equilibrium value. Two other energetically close singlet states and a quintet level are – again – coupled collisionally. In the line-formation region the departures from LTE are generally small. Non-LTE effects cannot affect the strongly populated lower levels as the corresponding radiative processes occur under optically thick conditions in the Lyman continuum. Radiative transitions are only effective for the N II 3s states and the levels above. We attribute the slight underpopulation of these levels at line-formation depths to these processes, resulting in an overpopulation of N III. A detailed analysis of the non-LTE effects is complicated by the small departures and they will be sensitive to small modifications in the entirety of the atomic data at this level. Additional investigations for N II should therefore be carried out for objects at higher temperatures.

The non-LTE abundance corrections for single spectral lines in our sample stars, as derived in Tables 5 and 6, are explained by the run of the departure coefficients and the corresponding line source function $S_{\rm L}$ for a given transition. In Fig. 6 the ratio of the line source function to

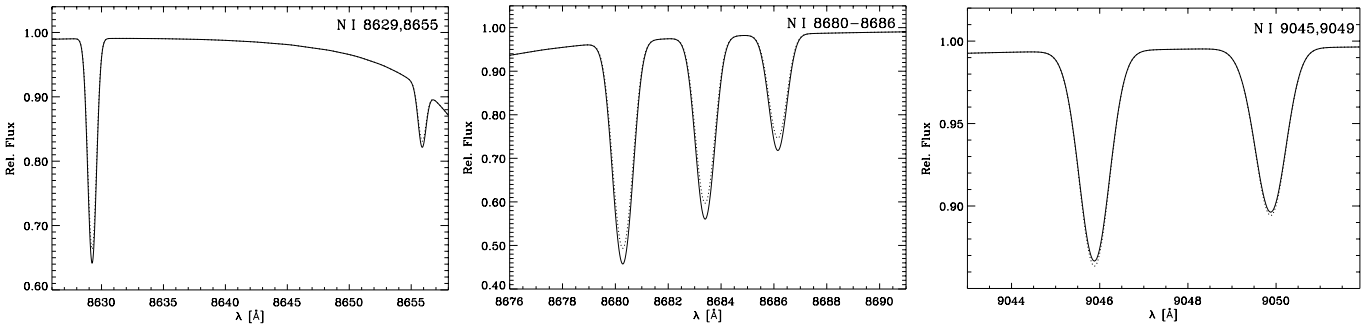

Fig. 7. Theoretical line profiles for the η Leo model (Sect. 4) with an increased microturbulence of $\xi = 10\,\mathrm{km\,s^{-1}}$. Solid line: statistical-equilibrium calculation with microturbulence included (Eq. (1)); dotted line: without microturbulence.

the Planck function B_ν for diagnostic lines for our models of η Leo and β Ori is displayed. A non-LTE strengthening of lines will occur in cases with a relative overpopulation of the lower level, a condition which is generally met at the formation depths of the observed N I/II lines. The run of S_L/B_ν as given for the η Leo model is typical for the other early A-type supergiants. Departures from unity set in deeper in the atmosphere for increasing T_eff and decreasing surface gravity; only small departures are therefore found in Vega, resulting in the much smaller non-LTE abundance corrections when compared to the supergiants. Typically, the – in the temperature range studied – weak N II lines are formed deeper in the atmosphere than the strong N I features.

3.2. Microturbulence

Microturbulence was originally introduced as a parameter to bring model calculations into better agreement with observation. The concept of some additional non-thermal line-broadening is not physically excluded, despite the lack of a comprehensive theoretical explanation for it at present.

Recently, McErlean et al. (1998) explicitly included microturbulence in the statistical-equilibrium calculations (with DETAIL, Eq. (1)) for helium in OB stars and find significantly different profiles as compared to the standard procedure of including microturbulence only in the final step of the spectrum synthesis (with SURFACE) for microturbulent velocities in excess of 10 km s^{-1}. Here we wish to investigate the contribution of this effect to the line-formation of N I/II. Note that the microturbulent velocities typically found in our test objects are comparable or even larger than the thermal velocity for nitrogen ($\sim$3.5 km s^{-1} at 10 kK).

This rather subtle effect depends on the details of the ionization balance and on the run of the departure coefficients for a given element (Paper I; Przybilla et al. 2001a, hereinafter Paper II). The lines of N I are expected to show some sensitivity to a non-zero microturbulence in the statistical-equilibrium calculations as the occupation numbers of the levels involved vary over the line-formation depths. Thus the radiative transitions occur under slightly different conditions as the formation depths of the line centres are pushed deeper into the atmosphere but simultaneously the frequency bandwidths for absorption are broadened by an increased microturbulent velocity. Changes in the non-LTE level populations and the line source functions vary in magnitude for different lines. Even lines too weak to react sensitively to microturbulence in the classical sense might therefore be affected.

In Fig. 7, test calculations for our model of η Leo with an increased microturbulence are displayed. For most of the N I lines a strengthening of up to 10% is found as ξ is increased from 0 to 10 km s^{-1} in the statistical-equilibrium computations within DETAIL. The line-formation itself is performed with SURFACE on the basis of the resulting population numbers for $\xi = 10$ km s^{-1} as in the classical approach. In general, the stronger lines are more sensitive. On the other hand, for some lines like N I $\lambda\lambda$ 9045-49 even a small weakening is found. The N II lines are unaffected, even in an analogous experiment for β Ori. For typical microturbulence values (<10 km s^{-1}) found in our sample stars, the magnitude of this effect is reduced but nevertheless should be accounted for in high S/N observations such as ours. We therefore use a consistent microturbulence in all our statistical-equilibrium and line-formation calculations in order to reduce the systematic error in the stellar parameter and abundance determination.

3.3. Comparison with other studies

The comparison of our model atom and the non-LTE departures with that of previous studies on N I will be instructive in explaining the large discrepancies, up to a factor of 2, in the derived nitrogen abundances for supergiants in particular, cf. Sect. 4.3.

Even for the main sequence star Vega all four studies on non-LTE effects in nitrogen, Takeda (1992), Rentzsch-Holm (1996, RH), Lemke & Venn (1996, LV) and the present work, find rather different departure coefficients – quantitatively as well as qualitatively. Takeda (1992) has compiled the most comprehensive N I model atom so far, with regard to the number of levels (119) and transitions (>2100) treated explicitly. Nevertheless,

Table 4. Basic properties and atmospheric parameters for the test stars.

HD	Name	Sp. Type	V (mag)	l (°)	b (°)	$v_{\rm rad}$ (km s^{-1})	$v \sin i$ (km s^{-1})	$T_{\rm eff}$ (K)	$\log g$ (cgs)	y	ξ (km s^{-1})	$\zeta_{\rm RT}$ (km s^{-1})
172167	α Lyr, Vega	A0 V	0.03	67.44	+19.24	−14	22	9550	3.95	0.09	2	0
							±2	±150	±0.1	±0.01	±0.5	+2
87737	η Leo	A0 Ib	3.52	219.53	+50.75	+3	9	9600	2.00	0.13	4	12
							±1	±150	±0.15	±0.02	±1	±2
111613	...	A2 Iabe	5.72	302.91	+2.54	−21	19	9150	1.45	0.105	7	21
							±3	±150	±0.15	±0.02	±1	±3
92207	...	A0 Iae	5.45	286.29	−0.26	−9	30	9500	1.20	0.12	8	20
							±5	±200	±0.15	±0.02	±1	±5
34085	β Ori, Rigel	B8 Iae:	0.12	209.24	−25.25	+21	36	12000	1.75	0.135	7	22
							±5	±250	±0.15	±0.02	±1	±5

the quality of the atomic data is lower than ours, as – except for the oscillator strengths and the photoionization cross-sections of the lowest three levels – only approximate data are used. By inspection of Takeda's Fig. 1 one might expect that the departure coefficients are too large, the model at solar metallicity already resembles ours to some point and the b_i increase enormously in the 1/10×solar model. Larger departure coefficients are also found by RH and LV, resulting in systematically larger non-LTE abundance corrections than in our work. Both model atoms resemble each other, with improved radiative data as compared to Takeda (1992) but still using only approximate collisional data. The number of line transitions is restricted in both studies, to 80 (RH) and 189 (LV) for a number of energy levels similar to that of the present work, as both use a complete linearisation scheme instead of the more powerful ALI technique, which allows us to treat ∼700 transitions in N I explicitly. The non-LTE effects in particular for neutral nitrogen seem to depend critically on accurate atomic data. All the previous studies struggle with difficulties to bring abundances from the doublet and quartet lines into accordance, indicating inaccurate collisional coupling between the two spin systems. This problem we can almost completely resolve with our model atom, with the one exception of the strongest observed line from the doublet spin system, N I λ8629, which we find to give a slightly low abundance. We cannot confirm the finding of LV, that Ly$_\alpha$ is of significant importance for the N I bound-bound rates: the "critical" N I resonance line in the Ly$_\alpha$ wing is optically thick throughout the atmosphere, implying a net radiative rate of practically zero.

The studies of Venn (1995b) and Takeda & Takada-Hidai (1995, TTH) apply the LV and Takeda (1992) models, respectively, to supergiants where the strengthened non-LTE will amplify the differences between the different models. Departure coefficients for N I levels in η Leo, the supergiant we have in common, are unfortunately not discussed. The non-LTE abundance corrections of TTH for the quartet lines agree to ∼0.2 dex with ours, but for the N I λ8629 doublet line TTH find a *positive* abundance correction; a second doublet line in their observations is unfortunately not analysed. Due to the breakdown of the pseudo-metastable character of the lower level of this transition and its sensitivity to even slight changes in the conditions of the calculations (cf. Sect. 3.1), TTH exclude this line from the abundance determination. Considering the more accurate atomic data in our study, we do not encounter such severe problems.

Venn (1995b) finds non-LTE abundance corrections systematically larger by ∼0.2–0.4 dex for η Leo, except for the only doublet line in her study, again N I λ8629, where $\Delta \log \varepsilon$ is almost identical with ours. The marked non-LTE strengthening in Venn's study has to be attributed to the large overpopulations of the 3s levels. In Venn's Fig. 8 departure coefficients for a supergiant at $T_{\rm eff} = 8400$ K and $\log g = 1.2$ (cgs) are displayed. We calculated N I populations with our model for the same parameters: Venn's departure coefficient for the 3s ^{2}P level is almost an order of magnitude larger at the maximum and for 3s ^{4}P Venn finds a continuous rise with decreasing optical depth to a much larger overpopulation, where we find a similar decrease as displayed in Fig. 5. The b_i of the other excited levels are also enhanced, but to a lesser degree, which might explain her larger non-LTE abundance corrections. Moreover, the three lowest-lying levels in Venn's calculation show a depopulation, while we find them to be in detailed equilibrium. In Venn's experiments, by modifying the collisional cross-sections, a solution is found which would bring her results into much better agreement with ours, cf. Sect. 5.3.2. in Venn (1995b). By artifically increasing the cross-sections to πa_0^2 (a_0 being the Bohr radius), Venn finds a reduction of the abundances from quartet lines on the order of 0.3 dex, while the doublet lines remain almost unaffected. Here, we have to re-emphasize the superior quality of the collisional excitation cross-sections used in our model atom, which ensures the accurate coupling of both spin systems.

A comparison of the non-LTE predictions from our N II model with those of Dufton & Hibbert (1981) and Becker & Butler (1989) cannot be carried out, as those studies concentrate on early B- and late O-type stars, close to the line-strength maximum for N II features, for which we have no observational material.

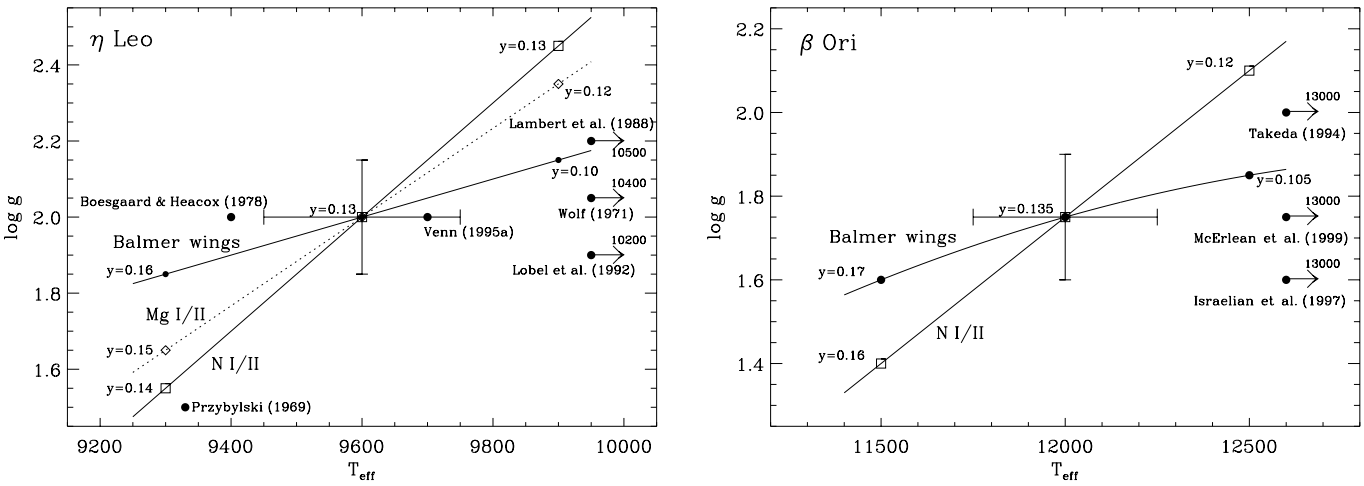

Fig. 8. Balmer line-wing and N I/II loci for the supergiants η Leo (left) and β Ori (right) on the temperature-gravity plane with the helium abundance y (by number) as an additional parameter. The adopted values for $T_{\rm eff}/\log g$ are shown with their estimated uncertainties. For η Leo, additional results as obtained from the Mg I/II ionization equilibrium (Paper II) are marked. Atmospheric parameters used in other analyses are also displayed: arrows indicate shifts in $T_{\rm eff}$ to the values cited.

Table 5. Abundance analysis for nitrogen in the A-type stars.

				α Lyr			η Leo			HD 111613			HD 92207		
λ (Å)	χ (eV)	$\log gf$	Acc.	W_λ(mÅ)	$\log\varepsilon$	$\Delta\log\varepsilon$	W_λ(mÅ)	$\log\varepsilon$	$\Delta\log\varepsilon$	W_λ(mÅ)	$\log\varepsilon$	$\Delta\log\varepsilon$	W_λ(mÅ)	$\log\varepsilon$	$\Delta\log\varepsilon$
N I:															
3830.43	10.69	−1.39	C+	...	...	...	S	8.37	−0.11	...	...	...	...	...	...
5999.43	11.60	−1.41	C+	...	...	...	5	8.49	−0.13	...	...	...	...	...	...
6008.47	11.60	−1.11	C+	...	...	...	10	8.52	−0.17	...	...	...	...	...	...
7423.64	10.33	−0.71	B+	17	7.66	−0.14	76	8.40	−0.48	87	8.45	−0.54	49	8.24	−0.55
7442.30	10.33	−0.38	B+	28	7.63	−0.16	130	8.39	−0.71	152	8.41	*−0.66*	80	8.19	−0.61
7468.31	10.34	−0.19	B+	44	7.68	−0.18	165	8.34	*−0.98*	197	8.46	*−0.81*	125	8.26	−0.69
7898.98	12.36	0.02	C	...	...	...	30	8.38	−0.31	19	8.35	−0.32	...	...	...
7899.28	12.36	−0.91	C												
8567.74	10.68	−0.66	B	S (15)	7.69	−0.22	S (95)	8.43	−0.44	S (85)	8.41	−0.47	S (40)	8.18	−0.52
8594.00	10.68	−0.33	B	S	7.65	−0.28	S (84)	8.36	*−0.93*	S	8.32	*−0.69*	...	...	...
8629.24	10.69	0.08	B	S (54)	7.56	−0.27	S (184)	8.14	*−0.86*	S (209)	8.18	*−0.69*	...	...	...
8655.88	10.69	−0.63	B	S	7.66	−0.29	S (72)	8.29	−0.51	S (57)	8.32	−0.46	...	...	...
8680.28	10.34	0.35	B+	S (105)	Blend	...	S (373)	8.48	*−1.71*	S (532)	8.53	*−1.38*	S	8.29	*−1.27*
8683.40	10.33	0.09	B+	S (72)	7.81	−0.26	S (312)	8.51	*−1.40*	S (408)	8.51	*−1.22*	S	8.26	*−0.96*
8686.15	10.33	−0.31	B+	S (39)	7.81	−0.18	S (215)	Blend	...	S	Blend	...	S	Blend	...
8703.25	10.33	−0.32	B+	S (50)	7.66	−0.15	211	8.55	*−0.94*	239	8.49	*−0.63*	123	8.27	−0.64
8711.70	10.33	−0.23	B+	S (53)	7.67	−0.17	228	8.47	*−1.02*	266	8.54	*−0.77*	155	8.21	−0.68
8718.84	10.34	−0.34	B+	S (37)	7.62	−0.12	198	8.50	*−0.92*	233	8.47	*−0.62*	122	8.29	−0.63
8728.90	10.33	−1.07	B+	...	...	...	S (63)	8.40	−0.34	S (63)	8.39	−0.34	...	...	...
9028.92	11.60	−0.13	B	...	...	...	S	8.39	−0.27	S	8.26	−0.36	...	...	...
9045.88	12.36	0.44	B	S (14)	7.64	−0.20	112	8.38	−0.49	S	8.38	−0.48	44	8.25	−0.56
9049.49	12.36	−0.86	B	S	7.66	−0.22	82	8.38	−0.43				S	8.31	−0.47
9049.89	12.36	0.28	B												
Mean					7.67	7.87		8.41	8.77		8.40	8.79		8.25	8.83
σ					0.07	0.09		0.09	0.16		0.10	0.13		0.04	0.08
N II:															
3995.00	18.50	0.21	B	...	...	...	10	8.32	−0.15	10	8.36	−0.18	15	8.28	−0.29
Mean					...	...		8.32	8.47		8.36	8.54		8.28	8.57
σ					...	...		...	...		...	...		...	...
N					7.67	7.87		8.40	8.74		8.40	8.76		8.25	8.81
σ					0.07	0.09		0.09	0.17		0.10	0.15		0.04	0.12

All gf values from Wiese et al. (1996). Accuracy indicators: A: 3%, B: 10%, C: 25%. Non-LTE abundances $\log\varepsilon$ are tabulated, $\Delta\log\varepsilon = \log\varepsilon_{\rm NLTE} - \log\varepsilon_{\rm LTE}$. Entries in *italics* are not used in the determination of means and standard deviations.

4. Application to observations

4.1. The spectra

As a test and first application of the model atom, nitrogen abundances for five objects are determined: the main sequence star Vega (HD 172167) and the supergiants η Leo (HD 87737), HD 111613, HD 92207 and β Ori (HD 34085). High S/N and high resolution Échelle spectra with a large wavelength coverage from the blue visual to the near-IR are used for this. The spectra were obtained with FEROS (Kaufer et al. 1999) at the ESO 1.52 m telescope in La Silla and FOCES (Pfeiffer et al. 1998) at the Calar Alto 2.2 m

telescope. Detailed information on the spectra and data processing for three of the stars are given in Paper II.

Two additional FEROS spectra are analysed in the present work. A 10 min exposure for HD 111613 was obtained during the observing run in January, 1999. We also selected a publicly available spectrum of β Ori (#0783, 20 s exposure), taken during commissioning in November, 1998. Both spectra were processed like the other FEROS data. A S/N of several hundred is achieved, like in the case of the other three sample stars.

4.2. Determination of stellar parameters

The accuracy of an abundance analysis critically depends on the determination of precise stellar parameters (see Sect. 2.4). A purely spectroscopic approach is chosen for the present work in order to prevent the restrictions encountered in any (spectro)photometric approach, namely inevitable extinction corrections and the lack of reliable photometric calibrations for the supergiants of interest.

For the supergiants, $T_{\rm eff}$ and $\log g$ are derived simultaneously by finding the ionization equilibrium of N I/II and by fitting the wings of the higher Balmer lines (typically from H_γ upwards). These are still formed in photospheric regions, in contrast to the H_α and H_β features which are affected by the stellar wind in supergiants. The profiles are calculated using the Stark broadening tables of Vidal et al. (1973). Non-LTE modelling of the He I lines is used to assess the stellar helium abundance $y = n(\mathrm{He})/[n(\mathrm{H})+n(\mathrm{He})]$. The stellar density structure responds to changes in the helium abundance because of its higher mean molecular weight (see e.g. Kudritzki 1973). $T_{\rm eff}$ and $\log g$ have to be appropriately adjusted at this point in some cases, see Fig. 8. The microturbulent velocity ξ is determined from non-LTE spectrum synthesis for a large ensemble of Fe II and Ti II lines by demanding that there is no relation between abundance and line strength. The metallicity [M/H] of the objects is determined from the mean of several elements with non-LTE abundance determinations (typically from O, Mg, S, Ti and Fe). Rotational velocities $v \sin i$ and macroturbulence $\zeta_{\rm RT}$ in the radial-tangential model are derived from the detailed synthesis of several spectral lines as both broadening mechanisms alter the line profile in different ways (Gray 1992). Usually, several iteration steps are necessary to obtain the final set of parameters. For Vega the widely used atmospheric model of Castelli & Kurucz (1994) is adopted, also calculated with the ATLAS9 code.

The basic properties and atmospheric parameters of the test stars are summarised in Table 4 with the estimated uncertainties. Information on the basic properties are adopted from the Simbad database at CDS (`http://cdsweb.u-strasbg.fr/ Simbad.html`).

The results match those obtained from the application of the Mg I/II ionization equilibrium (Paper II) except for one case: the low Mg I/II effective temperature (9100 K) for HD 92207 cannot be verified with the N I/II ionization equilibrium. We attribute this to inaccuracies in the ionizing radiation field longward of the Lyman jump, which trouble the Mg I ground state ionization but are not relevant in the case of N I with its higher ionization energy (cf. Sect. 2.3). Moreover, with the present parameters the agreement between the complete spectrum synthesis and the observations is improved. Nevertheless, in the case of the early A-type supergiants not too close to the Eddington limit, i.e. at luminosity classes below Ia, the Mg I/II ionization equilibrium appears to be a statistically more significant temperature indicator, as several lines in both ionization stages are available, in contrast to nitrogen, where only one N II line is strong enough to be observed. In the late B supergiant regime ionization equilibria of other elements, like O I/II, Al II/III, Si II/III or S II/III, can also be used. We derive an identical effective temperature for β Ori from the non-LTE ionization

Table 6. Abundance analysis for nitrogen in β Ori.

				β Ori		
λ (Å)	χ (eV)	$\log gf$	Acc.	W_λ (mÅ)	$\log\varepsilon$	$\Delta\log\varepsilon$
N I:						
7423.64	10.33	−0.71	B+	32	8.49	−0.51
7442.30	10.33	−0.38	B+	59	8.50	−0.60
7468.31	10.34	−0.19	B+	90	8.45	−0.68
8680.28	10.34	0.35	B+	S	8.62	*−1.38*
8683.40	10.33	0.09	B+	S	8.57	*−0.95*
8686.15	10.33	−0.31	B+	S	8.60	−0.67
8703.25	10.33	−0.32	B+	S	8.46	−0.58
8711.70	10.33	−0.23	B+	S	8.51	−0.61
8718.84	10.34	−0.34	B+	S	8.45	−0.56
9045.88	12.36	0.44	B	S	8.41	−0.61
9049.49	12.36	−0.86	B	S	8.48	−0.53
9049.89	12.36	0.28	B			
Mean					8.50	9.08
σ					0.07	0.09
N II:						
3955.85	18.47	−0.81	B	17	8.50	−0.18
3995.00	18.50	0.21	B	65	8.42	−0.45
4447.03	20.41	0.23	B	27	8.52	−0.26
4601.48	18.46	−0.43	B+	26	8.43	−0.24
4607.15	18.46	−0.51	B+	23	8.48	−0.22
4613.87	18.46	−0.67	B+	19	8.39	−0.21
4630.54	18.48	0.09	B+	S	8.49	−0.41
4643.09	18.48	−0.36	B+	S	8.54	−0.30
4788.14	20.65	−0.36	B	8	8.53	−0.09
4803.29	20.67	−0.11	B	15	8.61	−0.12
5045.10	18.46	−0.41	B+	25	8.57	−0.35
5666.63	18.47	−0.05	A	30	8.49	−0.37
5676.02	18.46	−0.37	A	19	8.50	−0.29
5679.56	18.48	0.25	A	51	8.60	*−0.54*
5686.21	18.47	−0.55	A	15	8.55	−0.29
5710.77	18.48	−0.52	A	16	8.59	−0.32
Mean					8.51	8.78
σ					0.06	0.11
N					8.51	...
σ					0.06	...

Table 7. Light element abundances for the sample stars.

Object	[He/H][a]	[C/H][b]	[N/H][c]	[O/H][a,d]	[CNO/H]
Vega	$+0.04 \pm 0.02$ (3)	-0.29 ± 0.11 (22)	$-0.25 \pm 0.07 \pm 0.14$ (14)	-0.24 ± 0.03 (10)	-0.26 ± 0.04
η Leo	$+0.19 \pm 0.04$ (14)	-0.52 ± 0.15 (7)	$+0.48 \pm 0.09 \pm 0.10$ (21)	-0.05 ± 0.05 (13)	-0.06 ± 0.05
HD 111613	$+0.08 \pm 0.05$ (10)	-0.33 ± 0.10 (5)	$+0.48 \pm 0.10 \pm 0.14$ (17)	-0.13 ± 0.04 (9)	-0.08 ± 0.04
HD 92207	$+0.15 \pm 0.04$ (10)	-0.19 (1)	$+0.33 \pm 0.04 \pm 0.14$ (12)	-0.04 ± 0.07 (6)	-0.04 ± 0.05
β Ori	$+0.20 \pm 0.04$ (15)	-0.37 ± 0.05 (3)	$+0.59 \pm 0.06 \pm 0.14$ (27)	-0.03 ± 0.05 (11)	$\pm 0.00 \pm 0.04$

[a] Paper IV; [b] Paper III; [c] this work; [d] Paper I.

equilibria of O I/II and S II/III using the merged model atoms of Paper I (O I) and Becker & Butler (1988; O II) and of Vrancken et al. (1996; S II/III).

Besides our own determinations of the stellar parameters for two of the supergiants, η Leo and β Ori, data have been obtained in several previous studies. For η Leo, Venn (1995a) finds a $T_{\rm eff}$ of 9700 ± 200 K and $\log g$ of 2.0 ± 0.2 (cgs) from spectroscopic indicators, viz H_γ wing fitting and the Mg I/II non-LTE ionization equilibrium, being in perfect agreement with our findings. Previous work on the stellar parameters of η Leo is summarized by Lobel et al. (1992), who also find ($10\,200 \pm 370$ K/1.9 ± 0.4) from a reanalysis of the photographic observations of Wolf (1971). The data are obtained by various techniques; to assess their accuracy we have to note that they are based on less elaborate (LTE) atmospheric models and on photographic plate observations, resulting in a wide spread. In addition to this, Lambert et al. (1988) use the values (10 500 K/2.2) for their analysis, without giving details of their derivation. The values reported by the different authors are marked in Fig. 8.

For β Ori two alternative groups of disjunct effective temperatures are found in the literature. The more recent determinations by McErlean et al. (1999), Israelian et al. (1997) and Takeda (1994) all agree on a $T_{\rm eff}$ of 13 000 K with $\log g$ varying between 1.6 and 2.1 (cgs). The former two studies adopt pure H+He non-LTE atmospheres for their analysis, thus neglecting the important line-blanketing, which will introduce a systematic shift in temperature. In the latter study the parameters are derived from photometric indicators (Balmer jump and the Paschen continuum gradient) and the H_γ and H_δ wings on the basis of a coarse grid of ATLAS6 atmospheres (Kurucz 1979). The high temperature value mostly results from the photometric indices, where inevitable corrections might result in a systematic shift. A number of studies derive the temperature directly from measured fluxes and interferometric stellar radius determinations or from the infra-red flux method. Lower temperatures have been found: $11\,550 \pm 170$ (Code et al. 1976), $11\,410 \pm 330$ (Beeckmans 1977), $12\,070 \pm 160$ (Stalio et al. 1977), 11 780 (Underhill et al. 1979), 11 014 (Blackwell et al. 1980), 11 380 (Underhill & Doazan 1982) and 11 023/11 453 (Glushneva 1985). Systematic errors will arise from inappropriate corrections for interstellar absorption. Indeed, of these, the only study that accounts for a non-zero E_{B-V} (Stalio et al. 1977, +0.04 vs. +0.05 as derived in Paper IV) finds a temperature in excellent accordance with our value.

4.3. Abundance analysis

The results of the abundance analysis for nitrogen are summarised in Table 5 and 6 which give the wavelength, excitation potential of the lower level and the adopted gf value for the observed lines, with accuracy indicators and sources for the gf values. Measured equivalent widths, derived non-LTE abundances

$$\log \varepsilon = \log \varepsilon_{\rm NLTE} = \log({\rm N/H}) + 12 \quad (3)$$

and non-LTE abundance corrections

$$\Delta \log \varepsilon = \log \varepsilon_{\rm NLTE} - \log \varepsilon_{\rm LTE} \quad (4)$$

for the different stars are also displayed. Blended lines are marked by "S" as long as an analysis via spectrum synthesis is still feasible. For lines originating in the hydrogen line wings the equivalent widths are measured against the local continuum (W_λ in parentheses). Non-LTE and LTE mean values and the line-to-line scatter (σ) are displayed separately for N I and N II, as is the combined nitrogen abundance. Note that the abundances are derived from the detailed spectrum synthesis and not from an equivalent-width study.

In Fig. 9 theoretical line profiles for the derived mean non-LTE nitrogen abundance are compared with the observations; excellent agreement is found for almost all lines. Discrepancies worth mentioning occur only for N I λ8629, the strongest line in the doublet spin system in the present study. N II λ4621 is strongly blended by a Fe II line with an apparently inaccurate gf-value, as the other N II lines of the same multiplet give consistent results. The lines in the A-type supergiants with $W_\lambda \gtrsim 300$ mÅ, typically the N I $\lambda\lambda$8680/83 features, also show an indication of the presence of an additional broadening process, probably connected to the hydrodynamical outflow at the base of the stellar wind, as the broadening becomes more pronounced for increasing mass-loss rates at comparable line strengths; the line depths, on the other hand, are well reproduced. By analysing only integrated quantities, i.e. equivalent widths, this problem will not be noticed and will lead to additional discrepancies between the weak and strong line analyses. For comparison, profiles from the mean LTE abundance are also shown, which give less satisfactory fits, most notably due to the systematic effects of non-LTE on the strongest lines. As some of the nitrogen lines are formed in the wings of H I lines,

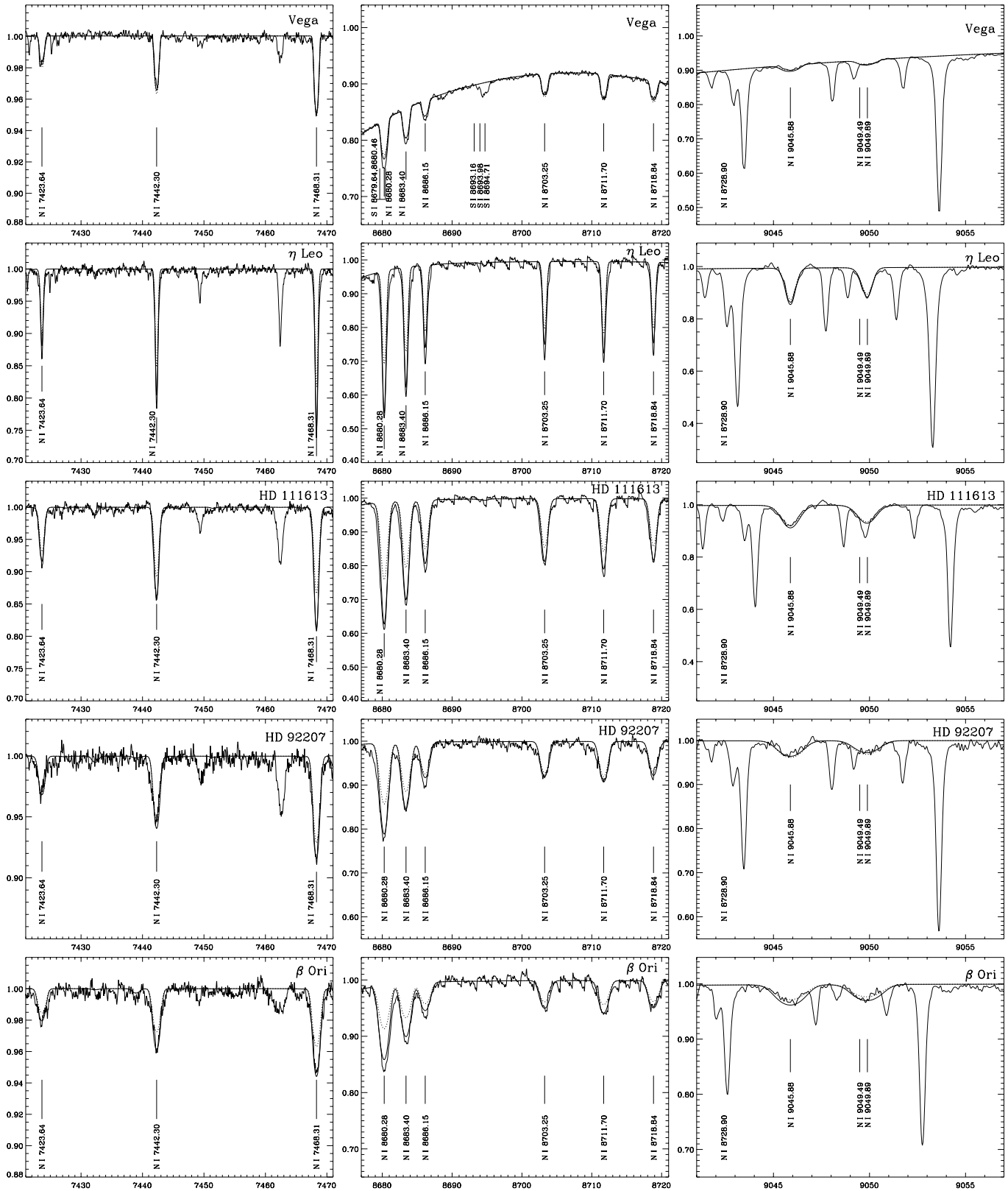

Fig. 9. Spectrum synthesis for selected N I/II lines in the test stars. Abscissa units are wavelengths in Å, ordinate is relative flux. Observed (thin solid) and computed (thick solid) non-LTE profiles for the mean nitrogen abundances in Tables 5 and 6 are displayed with line identifiers. Profiles for the appropriate LTE abundances are marked by a dotted line. Line formation for species other than H I, He I, C I/II, N I/II, O I/II, Mg I/II, S II/III, Ti II, Fe II is performed assuming LTE level populations (see Paper IV for details). The spectra in the red are contaminated by numerous sharp telluric lines and the FEROS data reduction is troubled by CCD fringes in the spectral region around 8700 Å. Note also, that the continuum in the red is often determined by the (overlapping) wings of the Paschen lines.

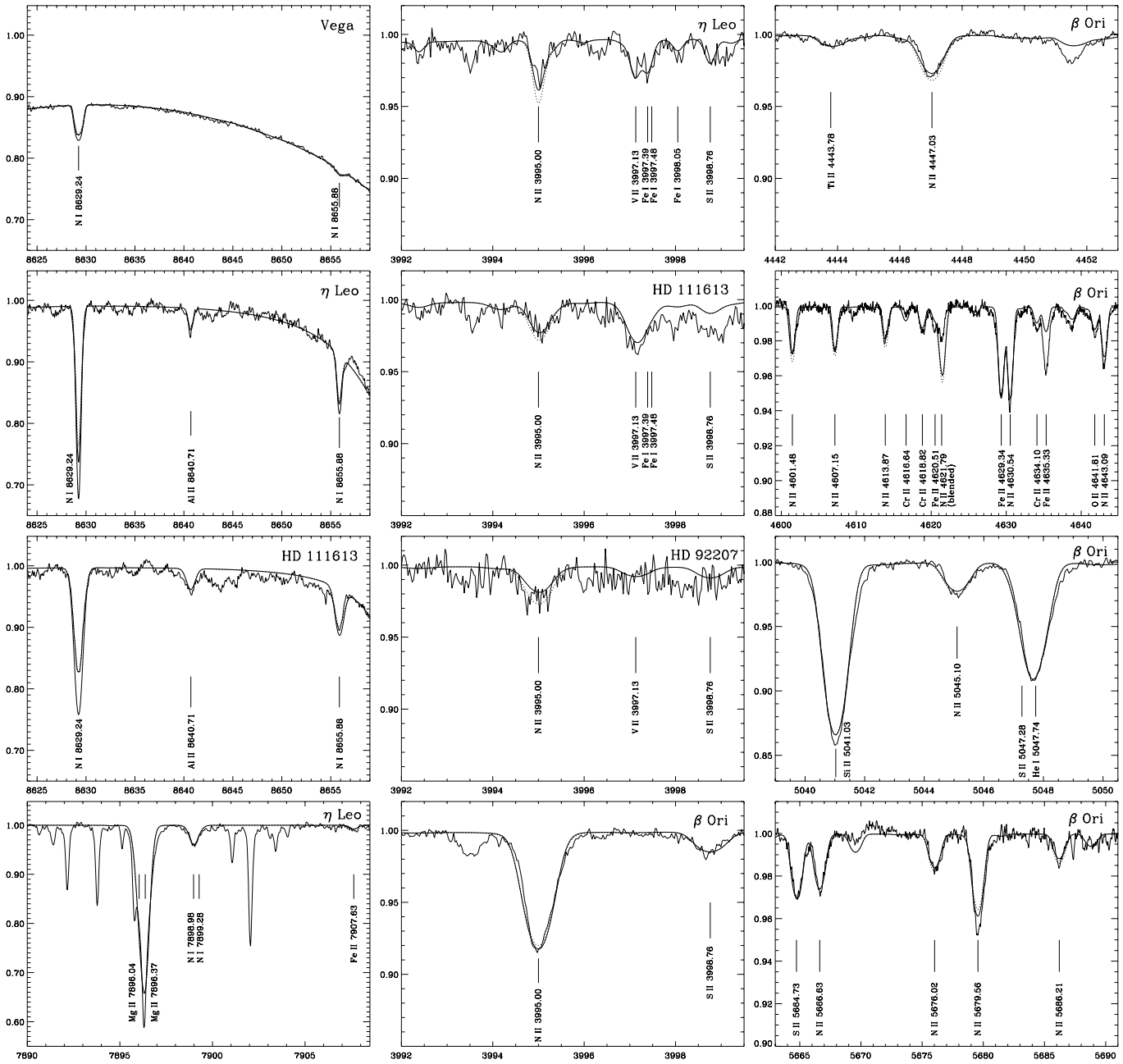

Fig. 9. continued.

profiles for hydrogen are calculated on the basis of non-LTE level populations and Stark profiles from Vidal et al. (1973), for the supergiants, and Stehlé & Hutcheon (1999), for the strongly overlapping Paschen lines in Vega. Apart from these, the following elements are treated in non-LTE to account for line blends: He I (Husfeld et al. 1989), C I/II (Paper III), O I/II (Paper I; Becker & Butler 1988), Mg I/II (Paper II), S II/III (Vrancken et al. 1996) and Ti II and Fe II (Becker 1998), with updated atomic data in several of the older models. The remaining elements with observed lines are included in LTE for the spectrum synthesis. This allows the reproduction of almost the entire observed spectral features. A detailed study of the test stars is performed elsewhere (Paper IV).

In Table 7 the results from the abundance analysis of the light elements (He, CNO) in the sample stars relative to the solar composition (Grevesse & Sauval 1998) are summarised, $[X/\mathrm{H}] = \log(X/\mathrm{H})_\star - \log(X/\mathrm{H})_\odot$, as needed in the subsequent discussion. We list the values obtained from the non-LTE analysis together with the 1σ-uncertainties from the line-to-line scatter and in the case of nitrogen also from the systematic errors, cf. Sect. 2.4, where the latter is the weighted (quadratic) mean from the contributions of N I and N II lines, respectively, to the total nitrogen abundance from both ionic species. The total number of analysed lines is given in parentheses. In the last column the sum of CNO in the sample stars relative to solar is diplayed.

Table 8. Comparison of N I/II abundance determinations for the test stars.

Source	$\log \varepsilon_{\rm LTE}$(N I)	$\log \varepsilon_{\rm LTE}$(N II)	$\log \varepsilon_{\rm NLTE}$(N I)	$\log \varepsilon_{\rm NLTE}$(N II)
		α Lyr		
This work	7.87 ± 0.09 (14)	...	7.67 ± 0.07 (14)	...
Lemke & Venn (1996)	7.97 ± 0.15 (8)	...	7.56 ± 0.05 (8)	...
Rentzsch-Holm (1996)	8.07 ± 0.22 (14)	...	7.77 ± 0.18 (14)	...
Takada-Hidai & Takeda (1996)	...	...	$\sim$7.5	...
Roby & Lambert (1990)	7.94 ± 0.11 (8)	...	...	...
Venn & Lambert (1990)	8.00 ± 0.03 (3)	...	...	...
Sadakane & Okyudo (1989)	7.85 ± 0.17 (6)	...	...	...
Lambert et al. (1982)	7.93 ± 0.15 (16)	...	...	...
		η Leo		
This work	8.77 ± 0.16 (12)	8.47 (1)	8.41 ± 0.09 (20)	8.32 (1)
Venn (1995b)	9.01 ± 0.10 (3)	...	8.09 ± 0.06 (8)	...
Takeda & Takada-Hidai (1995)	8.90 (1)	...	8.27 ± 0.03 (7)	...
Lambert et al. (1988)	9.0	...	...	...
		β Ori		
This work	9.08 ± 0.09 (9)	8.78 ± 0.11 (15)	8.50 ± 0.07 (11)	8.51 ± 0.06 (16)
Takeda & Takada-Hidai (1995)	9.16 ± 0.13 (5)	...	8.36 ± 0.07 (7)	...

Listed are the abundances with 1σ errors from the line-to-line scatter (number of lines analysed in parenthesis).

Non-LTE effects strengthen the N I/II lines systematically, thus the derived abundances decrease in comparison to LTE determinations. The N I lines around $\sim$8200 Å are not analysed here, due to the contamination of the spectral region by terrestrial H_2O lines and problems in the accurate determination of the local continuum, due to merging high Paschen lines/Paschen continuum.

Vega shows a nitrogen deficiency of 0.25 dex when compared to the solar abundance. This agrees well with the results for the other light elements and confirms similar findings by previous studies, but to a higher statistical significance. When compared to the general underabundance of the heavier elements by $\sim$0.5 dex, this pattern leads to the conclusion that Vega is a mild λ Bootis star (Venn & Lambert 1990). The non-LTE abundance corrections are moderate in this main sequence object, not exceeding 0.3 dex for single lines and being 0.2 dex in the mean.

In contrast, the four supergiants in our sample show nitrogen abundances $\sim$0.3–0.6 dex above solar. This finding is in excellent accord with the predictions of the new stellar evolution models accounting for rotation (Meynet & Maeder 2000; Heger & Langer 2000), especially, as carbon is found to be depleted in these objects and helium also enriched, with the sum of the CNO abundances remaining close to solar. CN-processed matter has apparently been mixed to the surface layers. The striking fact that the sample supergiant at lowest luminosity and therefore lowest mass, η Leo, shows one of the strongest nitrogen enrichments (and a corresponding carbon underabundance) indicates a blue-loop scenario for this star, with a first dredge-up N/C ratio, cf. the $9\,M_\odot$ – approx. η Leo's mass – evolutionary track of Meynet & Maeder (2000). On the other hand, the remaining three supergiants seem to have evolved directly from the main sequence, see Paper IV for a further discussion. A wide range in the non-LTE abundance corrections is found in the supergiants, for the strongest lines well in excess of 1 dex. Thus, reliable abundance analyses for this element cannot be performed under the assumption of LTE.

4.4. Comparison with other analyses

In the following our results for the sample stars are compared with those of other recent analyses. The abundance data are summarised in Table 8. Nitrogen abundances for HD 92207 and HD 111613 have been determined for the first time.

Vega Vega is an important photometric standard and has therefore been the subject of several abundance studies. The LTE abundances of practically all previous studies agree with our findings within the 1σ-errors; accounting for a higher $T_{\rm eff}$ (by 100 K) will bring the result of Venn & Lambert (1990) also into better agreement. This is not unexpected, as the stellar parameters and the gf-values used in the analyses are similar and the equivalent widths from the different measurements match well. The rather high abundance result of Rentzsch-Holm (1996) is derived from gf-values systematically smaller than those of our study, at almost identical stellar parameters.

Non-LTE abundances are determined in three other studies. Lemke & Venn (1996) find a slightly lower nitrogen abundance; in order to reduce their line-to-line scatter they exclude the doublet lines, as they find discrepancies in the non-LTE calculations between the doublet and quartet term systems. Rentzsch-Holm (1996) finds an nitrogen abundance larger than our value by 0.10 dex

with an enhanced statistical scatter. The only doublet line in that analysis also shows large inconsistencies to the quartet results (by almost 0.4 dex). Takada-Hidai & Takeda (1996) present corrections to the original work by Takeda (1992) where the influence of the Paschen lines on the formation of several N I lines in the near-IR was neglected, which resulted in a surprisingly low value of $\log\varepsilon \simeq 7.2$ instead of ∼7.5, as derived in the more recent work. However, Takada-Hidai & Takeda expect this to be also underestimated. In comparison, with our new model atom we find no discrepancies between the doublet and quartet spin system lines (we attribute this to the usage of accurate collisional data) and the statistical error is also reduced, also indicating an improvement.

η Leo This MK standard star has been included in two recent non-LTE studies on N I abundances in A-type supergiants by Venn (1995b) and Takeda & Takada-Hidai (1995). The differences in the non-LTE abundances, when compared with ours, might be explained in view of the diverse atomic models, cf. Sect. 3.3. No direct conclusions about the "true" nitrogen abundance can be drawn from this, but strong indication is given that our results are more relevant: more lines from both spin systems in N I and also from N II give consistent results.

In this case, the comparison of the LTE results is also very instructive. Only one weak line ($W_\lambda \leq 150$ mÅ) is present in the Takeda & Takada-Hidai (1995) study, N I λ8728. We adopt the corresponding LTE value for their LTE mean abundance for this star. Takeda & Takada-Hidai (1995) adopt different stellar parameters from the literature ($T_{\rm eff}$ = 10 200 K/$\log g$ = 1.90). Consequently they derive a slightly higher LTE N I abundance for similar gf-values and measured equivalent widths, which can be understood qualitatively. Venn on the other hand uses almost the same stellar parameters, (9700/2.0) vs. our (9600/2.0), with an identical microturbulence. Both sets of gf-values are almost identical and her equivalent widths are (except for one line) systematically smaller by ∼10%. From this, Venn's higher LTE abundance – by more than 70% – is surprising. However, when comparing only the three lines used by Venn in her LTE analysis this difference is reduced to 0.1 dex, which agrees within the corresponding uncertainties.

In addition, Lambert et al. (1988) analysed several N I lines of this supergiant in LTE for significantly different stellar parameters (10 500/2.2) and lower gf-values in the doublet spin system, cf. their Table 2, which qualitatively explains their higher abundance result.

β Ori The nitrogen abundance of the nearest late B-type supergiant has been determined in only one other study (Takeda & Takada-Hidai 1995). We have calculated mean LTE (only lines with $W_\lambda \leq 150$ mÅ) and non-LTE abundances (all lines) from their Table 4. In the comparison with our result the differences in the LTE abundances can be qualitatively explained by their choice of stellar parameters, $T_{\rm eff}$ =13 000 K and $\log g = 2.00$, with almost identical gf-values. Again, in non-LTE a higher abundance than ours should result but the opposite is found, which we attribute to fundamental differences in the model atoms, cf. Sect. 3.3.

5. Summary and conclusions

An extensive model atom for non-LTE line-formation calculations for neutral and singly-ionized nitrogen has been developed, based on the most accurate atomic data presently available. The ionization equilibrium of N I/II proves to be a reliable temperature indicator for late B-type and to some degree also for early A-type supergiants with distinct atmospheric nitrogen overabundances. Combined with Balmer-wing fitting this allows the determination of stellar parameters ($T_{\rm eff}/\log g$) with small uncertainties of typically 250 K/0.15 dex at $T_{\rm eff} \approx 12\,000$ K, comparable to or even better than those provided by conventional (spectro)photometric methods, for which reliable calibrations are largely lacking for supergiants. Uncertainties in nitrogen abundance determinations amount to typically 0.2 dex (random+systematical errors) for high-quality observations in main sequence objects and supergiants alike. For our test stars we derive the following nitrogen abundances:

Vega	$\log(\mathrm{N/H}) + 12 = 7.67 \pm 0.07 \pm 0.14$ (14)
η Leo	$\log(\mathrm{N/H}) + 12 = 8.40 \pm 0.09 \pm 0.10$ (21)
HD 111613	$\log(\mathrm{N/H}) + 12 = 8.40 \pm 0.10 \pm 0.14$ (17)
HD 92207	$\log(\mathrm{N/H}) + 12 = 8.25 \pm 0.04 \pm 0.14$ (12)
β Ori	$\log(\mathrm{N/H}) + 12 = 8.51 \pm 0.06 \pm 0.14$ (27).

The nitrogen underabundance by 0.25 dex in Vega supports the claims for a deficit of the light elements by ∼0.3 dex in this star, in contrast to the ∼0.5 dex underabundance of the refractory (α- and iron-peak) elements, which lead to the conclusion that Vega is a mild λ Bootis star. In the sample supergiants, we find nitrogen overabundances by ∼0.3–0.6 dex, which in view of accompanying carbon underabundances – with the sum of the carbon and nitrogen abundances staying close to solar – indicates the presence of CN-cycled matter in the atmospheric layers. This observational finding is in excellent accord with the predictions of the new stellar evolution calculations accounting for mass-loss and rotation. Our model results match the observed profiles well.

In comparison with previous non-LTE studies on N I, in particular for supergiants, we find significantly higher abundances, up to a factor of 2. This has a large impact on the interpretation of the evolutionary status of such stars, when compared with stellar evolution models. We obtain our conclusions from observational material at higher S/N and larger wavelength coverage (i.e. more lines are available) and from a model atom accounting for improved atomic data; consistent results are derived from N I lines of the doublet and quartet spin systems alike – avoiding the inconsistencies found in the previous studies – and from N II lines.

In a main sequence star like Vega, the non-LTE abundance corrections for N I lines are below 0.3 dex. This changes drastically for supergiants, where atmospheric nitrogen overabundances produce strong lines, with line formation regions extending over considering parts of the atmosphere where departure coefficients deviate significantly from unity. Non-LTE abundance corrections in excess of 1 dex are found in some cases. N II lines are observable in the supergiants due to the nitrogen overabundances and are otherwise absent in late B- and early A-type stars; abundance corrections for this ionic species amount to $\lesssim$0.5 dex in the mean. Both, N I and N II lines are strengthened systematically in non-LTE. The nature of the non-LTE effects is well understood for N I but for N II the smallness of the non-LTE departures complicates the identification of the responsible effects. A strong sensitivity of the N I lines to changes in the collisional excitation data is found. Accurate energy-dependent collision strengths for a large number of transitions are used for the first time.

Subtle effects are evoked by the inclusion of the microturbulence parameter in the statistical-equilibrium calculations for N I/II. In contrast to the standard approach – accounting for microturbulence only in the line formation – even weak lines might be affected by modified level populations. N I lines are strengthened in most cases while the N II lines are unaffected. This can result not only in different abundances but – when using the N I/II ionization equilibrium as a temperature indicator – also in modified stellar parameters. The effect is small but cannot be neglected for high quality observations.

Acknowledgements. We are grateful to A. Kaufer for his help in obtaining some of the spectra at La Silla and to S. Tubbesing for his aid with the data reduction. Our work has benefitted from the beautiful spectrum of Vega contributed by A. Korn. We would further like to thank R. M. Frost for providing extended tabulations of collisional data in digital form and K. A. Venn and Y. Takeda for clarifying comments and J. Puls for helpful discussions. This research has made use of the Simbad database, operated at CDS, Strasbourg, France.

References

Allen, C. 1973, Astrophysical Quantities, 3rd ed. (Athlone Press, London)
Aufdenberg, J. P. 2000, Ph.D. Thesis, Arizona State University
Becker, S. R. 1998, in Boulder-Munich II: Properties of Hot, Luminous Stars, ed. I. D. Howarth (San Francisco: ASP)
Becker, S. R., & Butler, K. 1988, A&A, 201, 232
Becker, S. R., & Butler, K. 1989, A&A, 209, 244
Beeckmans, F. 1977, A&A, 60, 1
Blackwell, D. E., Petford, A. D., & Shallis, M. J. 1980, A&A, 82, 249
Boesgaard, A., & Heacox, W. 1978, ApJ, 226, 888
Bresolin, F., Kudritzki, R. P., Méndez, R. H., & Przybilla, N. 2001, ApJ, 548, L159
Brook, E., Harrison, M. F. A., & Smith, A. C. H. 1978, J. Phys. B, 11, 3115
Butler, K., & Giddings, J. 1985, Newsletter on Analysis of Astronomical Spectra No. 9, University of London
Castelli, F., & Kurucz, R. L. 1994, A&A, 281, 817
Code, A. D., Davis, J., Bless, R. C., & Hanbury Brown, R. 1976, ApJ, 203, 417
Cowley, C. 1971, Observatory, 91, 139
Cunto, W., & Mendoza, C. 1992, Rev. Mex. Astrofis., 23, 107
Dufton, P. L., & Hibbert, A. 1981, A&A, 95, 24
Frost, R. M., Awakowicz, P., Summers, H. P., & Badnell, N. R. 1998, J. Appl. Phys., 84, 2989
Giddings, J. R. 1981, Ph.D. Thesis, University of London
Gies, D. R., & Lambert, D. L. 1992, ApJ, 387, 673
Glushneva, I. N. 1985, in Calibration of fundamental stellar quantities, ed. D. S. Haynes, N. E. Pasinetti, & A. G. Davis Philip, IAU Symp. 111
Gray, D. F. 1992, The observation and analysis of stellar photospheres, 2nd ed. (Cambridge University Press)
Grevesse, N., & Sauval, A. J. 1998, Space Sci. Rev., 85, 161
Griem, H. R. 1964, Plasma Spectroscopy (McGraw-Hill Book Company, New York)
Griem, H. R. 1974, Spectral Line Broadening by Plasmas (Academic Press, New York and London)
Heger, A., & Langer, N. 2000, ApJ, 544, 1016
Henry, R. J. W. 1970, ApJ, 161, 1153
Herrero, A., Corral, L. J., Villamariz, M. R., & Martin, E. L. 1999, A&A, 348, 542
Herrero, A., Kudritzki, R. P., Vilchez, J. M., et al. 1992, A&A, 261, 209
Herrero, A., Puls, J., & Villamariz, M. R. 2000, A&A, 354, 193
Hofsäß, D. 1979, Atomic Data and Nuclear Data Tables, 24, 285
Hubeny, I., & Lanz, T. 1993, in Peculiar Versus Normal Phenomena in A-Type and Related Stars ed. M. M. Dworetsky, F. Castelli, & R. Faraggiana (San Francisco: ASP)
Husfeld, D., Butler, K., Heber, U., & Drilling, J. S. 1989, A&A, 222, 150
Israelian, G., Chentsov, E., & Musaev, F. 1997, MNRAS, 290, 521
Johansson, S., & Leckrone, D. S. 1996, in Model Atmospheres and Spectrum-Synthesis, ed. S. J. Adelman, F. Kupka, & W. W. Weissed (San Francisco: ASP)
Kaufer, A., Stahl, O., Tubbesing, S., et al. 1999, The ESO Messenger, 95, 8
Kilian, J. 1992, A&A, 262, 171
Kudritzki, R. P. 1973, A&A, 28, 103
Kudritzki, R. P. 1988, in 18th Advanced Course of the Swiss Society of Astrophysics and Astronomy (Saas-Fee Courses): Radiation in Moving Gaseous Media, Geneva Observatory, ed. Y. Chmielewski, & T. Lanz
Kurucz, R. L. 1979, ApJS, 40, 1
Kurucz, R. L. 1991, in Stellar Atmospheres: Beyond Classical Models, ed. L. Crivellari et al., NATO ASI Ser. C-152, 441
Kurucz, R. L. 1992, Rev. Mex. Astrofis., 23, 45
Lambert, D. L., Hinkle, K. H., & Luck, R. E. 1988, ApJ, 333, 917
Lambert, D. L., Roby, S. W., & Bell, R. A. 1982, ApJ, 254, 663
Lemke, M., & Venn, K. A. 1996, A&A, 309, 558
Lennon, D. J. 1994, Space Sci. Rev., 66, 127
Lennon, D. J., Dufton, P. L., & Fitzsimmons, A. 1993, A&AS, 97, 559
Lobel, A., Achmad, L., de Jager, C., & Nieuwenhuijzen, H. 1992, A&A, 256, 159

Luo, D., & Pradhan, A. K. 1989, J. Phys. B, 22, 3377
Lyubimkov, L. S. 1991, in Evolution of Stars: The Photospheric Abundance Connection, ed. G. Michaud, & A. Tutukov (Dordrecht: Kluwer)
Maeder, A., & Meynet, G. 2001, A&A, 373, 555
McErlean, N. D., Lennon, D. J., & Dufton, P. L. 1998, A&A, 329, 613
McErlean, N. D., Lennon, D. J., & Dufton, P. L. 1999, A&A, 349, 553
Meynet, G., & Maeder, A. 2000, A&A, 361, 101
Mihalas, D. 1978, Stellar Atmospheres (2nd ed.) (W. H. Freeman and Company, San Francisco)
Moore, C. E. 1993, in CRC Handbook of Chemistry and Physics, 76th ed., Boca Raton: CRC, ed. J. W. Gallagher
Pfeiffer, M. J., Frank, C., Baumüller, D., et al. 1998, A&AS, 130, 381
Przybilla, N. 1997, Diplomarbeit, Ludwig Maximilians Universität, München
Przybilla, N., Butler, K., Becker, S. R., Kudritzki, R. P., & Venn, K. A. 2000, A&A, 359, 1085 (Paper I)
Przybilla, N., Butler, K., Becker, S. R., & Kudritzki, R. P. 2001a, A&A, 369, 1009 (Paper II)
Przybilla, N., Butler, K., Becker, S. R., & Kudritzki, R. P. 2001b, in preparation (Paper IV)
Przybilla, N., Butler, K., & Kudritzki, R. P. 2001c, A&A, 379, 936 (Paper III)
Przybylski, A. 1969, MNRAS, 146, 71
Rentzsch-Holm, I. 1996, A&A, 305, 275
Roby, S. W., & Lambert, D. L. 1990, ApJS, 73, 67
Rybicki, G. B., & Hummer, D. G. 1991, A&A, 245, 171
Sadakane, K., & Okyudo, M. 1989, PASJ, 41, 1055
Seaton, M. J. 1962, in Atomic and Molecular Processes (Academic Press, New York)
Seaton, M. J., Yu Y., Mihalas, D., & Pradhan, A. K. 1994, MNRAS 266, 805
Stalio, R., Selvelli, P. L., & Crivellari, L. 1977, A&A, 60, 109
Stehlé, C., & Hutcheon, R. 1999, A&AS, 140, 93
Takada-Hidai, M., & Takeda, Y. 1996, PASJ, 48, 739
Takeda, Y. 1992, PASJ, 44, 649
Takeda, Y. 1994, PASJ, 46, 181
Takeda, Y., & Takada-Hidai, M. 1995, PASJ, 47, 169
Underhill, A. B., Divan, L., Prévot-Burnichon, M.-L., & Doazan, V. 1979, MNRAS, 189, 601
Underhill, A., & Doazan, V. 1982, B stars with and without emission lines, NASA SP-456
Van Regemorter, H. 1962, ApJ, 136, 906
Venn, K. A. 1995a, ApJS, 99, 659
Venn, K. A. 1995b, ApJ, 449, 839
Venn, K. A. 1999, ApJ, 518, 405
Venn, K. A., & Lambert, D. L. 1990, ApJ, 363, 234
Venn, K. A., Lennon, D. J., Kaufer, A., et al. 2001, ApJ, 547, 765
Venn, K. A., McCarthy, J. K., Lennon, D. J., et al. 2001, ApJ, 541, 610
Vidal, C. R., Cooper, J., & Smith, E. W. 1973, ApJS, 25, 37
Vrancken, M., Butler, K., & Becker, S. R. 1996, A&A, 311, 661
Wiese, W. L., Fuhr, J. R., & Deters, T. M. 1996, J. Phys. & Chem. Ref. Data, Mon. 7
Wolf, B. 1971, A&A, 10, 383
Yamada, I., Danjo, A., Hirayama, T., et al. 1989, J. Phys. Soc. Jpn., 58, 1585